European Commission
Research Programme of the Research Fund for Coal and Steel

ANGELHY

Innovative solutions for design and strengthening of telecommunications and transmission lattice towers using large angles from high strength steel and hybrid techniques of angles with FRP strips

WORK PACKAGE 4 – DELIVERABLE 4.1

Parametric models of case studies and loads

Coordinator:

National Technical University of Athens - NTUA, Greece

Beneficiaries:

ArcelorMittal Belval & Differdange SA - AMBD, Luxembourg

Universite de Liege - ULG, Belgium

COSMOTE Kinites Tilepikoinonies AE - COSMOTE, Greece

Centre Technique Industriel de la Construction Metallique - CTICM, France

SIKA France SAS - SIKA, France

Grant Agreement Number: 753993

29/12/2020

AUTHORS:

NATIONAL TECHNICAL UNIVERSITY OF ATHENS
Institute of Steel Structures
Iroon Polytechniou 9, 15780 Athens, Greece
Authors: Dimitrios V. Bilionis, Konstantinos Vlachakis, Dimitrios Vamvatsikos

TABLE OF CONTENTS

1 Introduction

Task 4.1 of the ANGELHY was associated with the probabilistic modelling of the structure and loads of steel lattice towers. To do so, various parametric models of the towers considered in WP 1 were developed. Herein, the selected models of the telecommunication and transmission towers will be presented. In specific, three different types of towers were considered: a telecommunication tower, a suspension transmission tower and a dead-end transmission tower.

All three towers were analysed in four different configurations summarised in Table 1.1: a) an initial design according to EN standards using conventional steel, b) a corroded version of (a) due to ageing effect at the end of its expected service life (assumed to be 60 years), c) a strengthened version of (b) with hybrid members strengthened via FRP plates and d) a redesigned tower, having the same geometry as the initial tower, but with High Strength Steel (HSS) members. The only exception in the above was the case of the suspension transmission tower where the analysis of version (c) was skipped.

Based on the above, the purpose of this deliverable is to provide a detailed description of all the versions of the three towers examined in this task, along with all the corresponding assumptions regarding their structural parameters and assigned loads.

Table 1.1: Types of Lattice Towers Considered

Telecommunication Tower	**Suspension Transmission Tower**	**Dead-End Transmission Tower**
Initial State	Initial State	Initial State
Corroded State	Corroded State	Corroded State
Strengthened Hybrid	-	Strengthened Hybrid
High Strength Steel (HSS) tower	High Strength Steel (HSS) tower	High Strength Steel (HSS) tower

2 Telecommunication Tower

2.1 Structural description and modelling

2.1.1 Geometry

The lattice tower of the study is 51m high and is square in plan [1]. The tower is divided in 3 parts. The first part from the basis up to 24m has trapezoidal shape, the second part between 24 and 48 m rectangular shape, while the top part from 48 to 51m triangular shape. Figure 2.1 shows a side view and plan views of the tower. The tower has horizontal diaphragms every 3 meters along its height (Figure 2.1b). It also includes five working platforms at heights of 12, 24, 42 and 45m (Figure 2.1c). In the middle of the tower run a ladder and a waveguide rack for the cables of the antennas and are supported by the horizontal diaphragms.

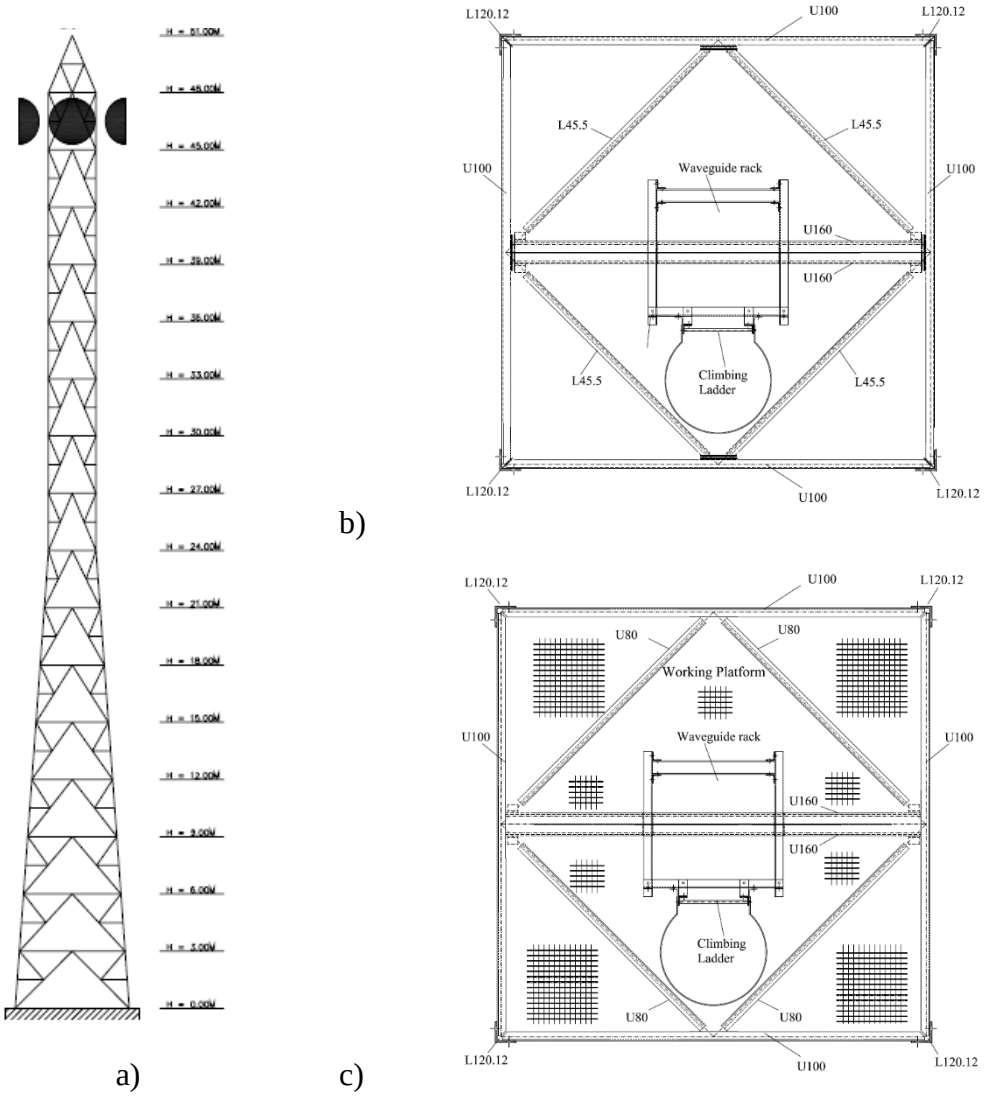

Figure 2.1: a) Side view of the tower. b) Typical plan of a horizontal diaphragm. c) Typical plan of a working platform [1].

The main structural members, legs and bracing elements, are composed of angle cross sections, while the members of the diaphragms and platforms of channel sections. The bracing pattern is composed of primary and secondary bracing members as illustrated in Figure 2.2.

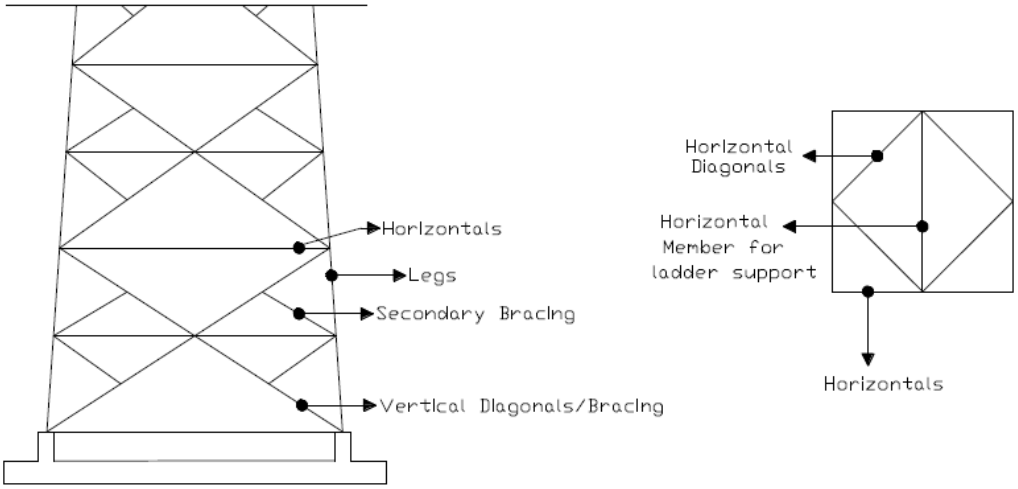

Figure 2.2: Designation of structural members [1].

2.1.2 Material properties

The structural steel grade was S235 for all tower members. Since the purpose of this investigation is not the design but a performance assessment for the lattice tower, the actual values of the steel mechanical properties (as proposed in the literature) were assumed in the analysis, instead of the nominal ones. Specifically, for steel grade S235 the values of 328.80MPa and 435.41MPa were adopted as the yield and respectively ultimate stress [2]. The material stress-strain curve that was assumed in the analysis is presented in Figure 2.3. The value of E corresponds to the elastic modulus of steel, set equal to 210 GPa, while the buckling reduction factor χ was calculated for each structural member according to EN 1993-3-1 [3] to reduce its compression strength. Since the members of the tower have different cross-sections, the stress-strain curve is different for each member and thus Figure 2.3 presents only the general form of the stress-strain curve for all members.

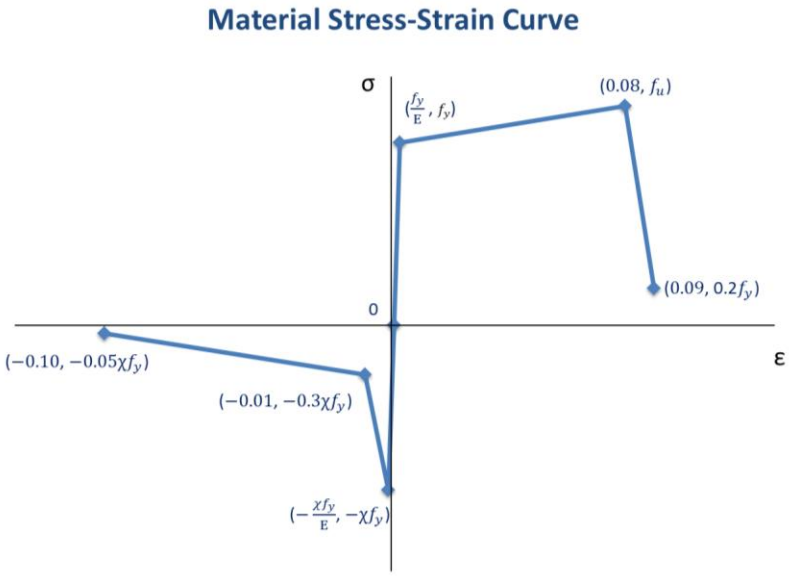

Figure 2.3: General form of a member stress-strain curve

2.2 Loads

2.2.1 Gravity Loads

The self-weight of the tower members is calculated considering the unit weight of steel equal to 78.50 kN/m^3. The weight of the climbing ladder is taken as 15.30 kN and the weight of the waveguide rack 14.60 kN. Four parabolic antennas are installed at the top (height 45-48m) of the tower. Each parabolic antenna has a weight of 2.30 kN. The weight of the cables is assumed to be 0.05 kN/m per antenna. Finally, the weight of the five working platforms is considered as 0.25 kN/m^2.

The live load of the climbing ladder is 5.00 kN, while the live load at the working platforms is assumed to be 2.00 kN/m^2.

2.2.2 Wind Loads

In the case of a telecommunication tower with parabolic antennas, the total wind force acting on the structure consists of two main components, namely the force acting on the tower (i.e. the structural members) and the force acting on the parabolic antennas [4]:

$$F_T = F_{tower} + F_{antennas} \quad \text{Eq. 2.1}$$

2.2.2.1 Wind Force at Tower

The wind force acting on the tower is calculated by the Equation:

$$F_{tower} = qC_D A_{ref} \quad \text{Eq. 2.2}$$

where:

q is the dynamic pressure of the wind, C_D is the drag coefficient and A_{ref} is the area of the members projected normal to the level of the wind.

The dynamic pressure of the wind q depends on the air density ρ and the wind speed u and is estimated using the following Equation:

$$q = \frac{1}{2}\rho u^2 \quad \text{Eq. 2.3}$$

Herein, ρ was assumed to be equal to 1.25 kg/m^3.

The drag coefficient C_D for lattice steel structures depends on the solidity ratio φ. According to EN1991-1-4 [5], the solidity ratio φ is the fraction of the sum of the projected area A of the members of the structure's face normal to that face divided by the total enclosed area A_c by the face's boundaries projected normal to that face. Thus:

$$\varphi = \frac{A}{A_c} \quad \text{Eq. 2.4}$$

Herein, the structure was divided into sixteen segments (every 3 m) along its height considering each horizontal diaphragm to be at the middle of the segment. For each segment the solidity ratio was calculated and the corresponding drag coefficient was estimated based on [5]. Finally, the forces of each segment were assigned to the level of the corresponding diaphragm.

2.2.2.2 Wind Force at the Parabolic Antennas

According to [6], the commonly used practice in the past for the estimation of the wind force on parabolic antennas was to calculate the drag coefficient of the isolated antenna, then the corresponding force, and finally adding the result to the force of the tower as calculated by Eq. (2.2). However, this practice would overestimate the total force since the antenna may shield part of the tower. This is also evident in case of multiple antennas installed on the tower. For this reason, except for the drag coefficient of the isolated antenna, an additional interference factor was added in the load calculation. Thus, the wind force, in case of two identical in size antennas installed on the same height at the tower, is calculated as follows [4],[7]:

$$F_{antennas} = qA_a(C_{Da_1}f_{a_1} + C_{Da_2}f_{a_2}) \quad \text{Eq. 2.5}$$

where:

q is the dynamic pressure of the wind, A_α is the area of each antenna projected normal to the level of the wind, $C_{D\alpha1}$ and $C_{D\alpha2}$ are the drag coefficients for the two isolated antennas and $f_{\alpha1}$ and $f_{\alpha2}$ are the corresponding interference factors for each of the antennas.

The values of the drag coefficients and the interference factors of the antennas are mainly based on the wind angle and the solidity ratio. Those values are usually estimated experimentally [4],[7],[8]. Herein, in lack of experimental results for the tower and the antennas, proposed values by an experimental study of a similar case [7] for $C_{D\alpha1}$, $C_{D\alpha2}$, $f_{\alpha1}$ and $f_{\alpha2}$ were adopted.

2.2.2.3 Wind Speed Profile

Wind speed increases with height following a specific pattern known as wind speed profile. Herein, a power law wind speed profile was considered. According to the power law profile, the value of wind speed at a height z is given by:

$$\frac{u}{u_{ref}} = \left(\frac{z}{z_{ref}}\right)^{a} \quad \text{Eq. 2.6}$$

where:

u is the wind speed at height z (in m/s), u_{ref} is the wind speed at a reference height z_{ref} (in m/s) and α is the power law exponent. In this work, a power law exponent α=0.20 was used, as proposed by IEC 61400-1 [9] for onshore structures.

Eq. (2.6) gives the values of the wind speed along the height of the tower. Herein, the values of wind speed at the heights of the horizontal diaphragms and the center of the parabolic antennas were calculated. Based on these values, the wind force along the height of the tower is estimated by applying Eq. (2.1).

The wind speed and the wind force profiles are presented in Figure 2.4. It can be inferred that both profiles follow a similar pattern. The only difference is observed at the heights of the parabolic

antennas. This is due to the additional force that is added to the tower by the parabolic antennas as expressed in Eq. (2.5).

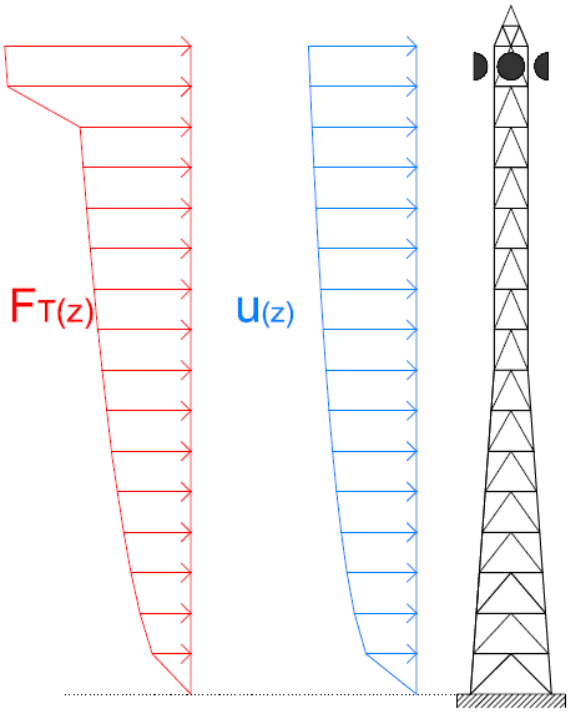

Figure 2.4: Wind speed *u(z)* and wind force $F_T(z)$ profiles

2.2.2.4 Wind Field Simulation

The simulation of the wind field where the tower is placed was performed in TurbSim software [10]. TurbSim has been developed by National Renewable Energy Laboratory of the USA and is mainly used in wind industry applications. The software simulates a 2D wind field as shown in the Figure 2.5a. TurbSim can also generate time histories of wind speed over a user-defined period (e.g. 10 min, 1 hour etc.) and for a specific wind speed value which is considered to be the mean wind speed (reference wind speed). The wind field is defined by a custom grid whose dimensions and resolution are specified by the user. The software finally outputs the corresponding time histories of the values of the three wind speed components (for each of the three directions X, Y, Z) at the points of the grid of the wind field (Figure 2.5b). For each of those components the corresponding wind force time histories (mainly for the directions X and Y, since the component of direction Z is ignored in this study) were estimated by applying Eq. (2.2) for the wind force at the tower and Eq. (2.5) for the wind force at the antennas.

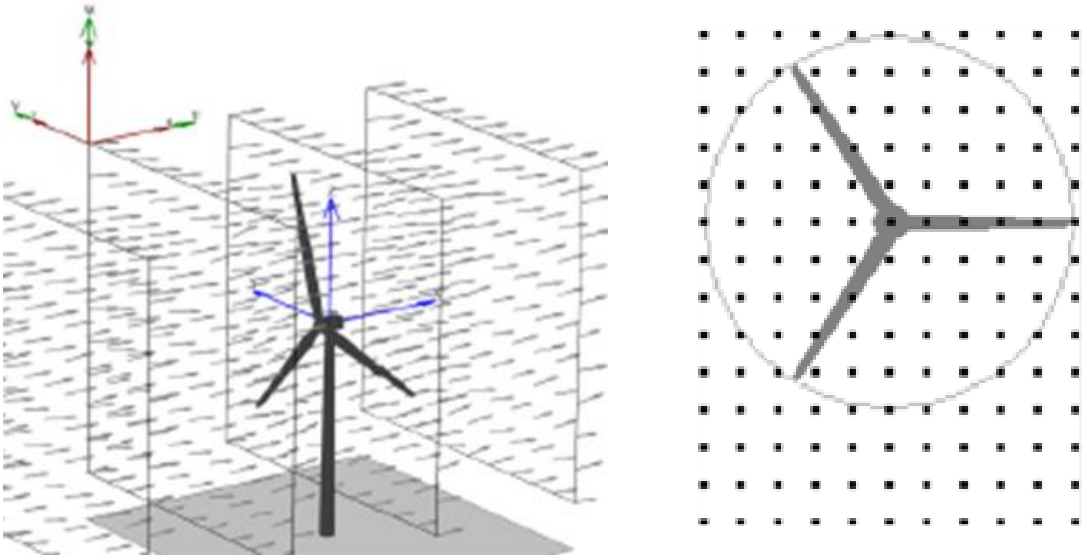

a) b)

Figure 2.5: a) 2D wind field created in TurbSim. b) Grid points of the wind field where simulated wind speed values are reported (adopted by [10]).

2.2.3 Ice Loads

Apart from wind, another environmental hazard which should be taken into account is ice. In the case of a lattice telecommunication tower, ice is accumulated on the surface of the structural members and the parabolic antennas. Ice accretion affects the loads of the structure in two major ways. First, the weight (i.e. dead load) of the members and the parabolic antennas increase and secondly, the projected area of the members and the antennas also increase. Following the previous section, where the estimation of the wind loads was discussed, it can be inferred that an increase in the projected area of the members affects the solidity ratio of the tower and the corresponding drag coefficients resulting in a larger wind force for the same wind speed value.

Herein, it was assumed that an ice layer of uniform thickness was formed on the surface of the exposed parts of the members and the parabolic antennas. Figure 2.6 presents the form of ice accretion and its area for each type of the steel cross section used in the current structure and the parabolic antennas. Finally, it should be noted that the unit weight of ice was considered equal to 7.00 kN/m^3.

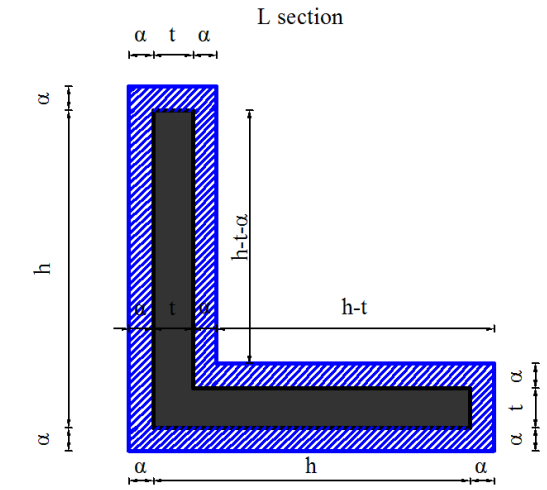

Ice Area:
$A_{ice} = \alpha(t + 2a) + ah + a(h + 2a) + at + a(h - t + a) + a(h - t - a)$

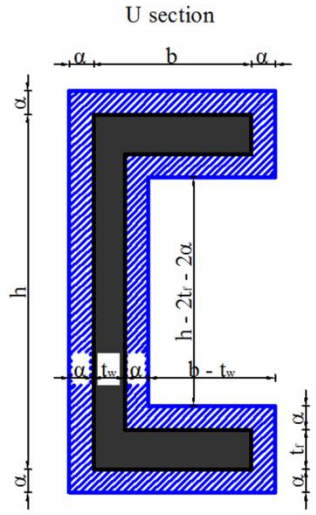

Ice Area:
$A_{ice} = 2\alpha(b + 2a) + 2a(b + a - t_w) + a(h - 2t_f - 2a) + ah + 2at_f$

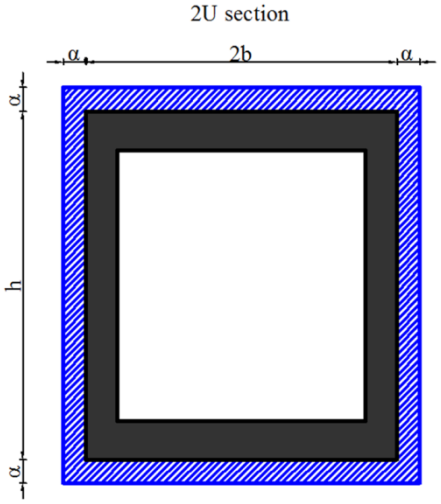

Ice Area:
$A_{ice} = 2\alpha(2a + 2b) + 2ah$

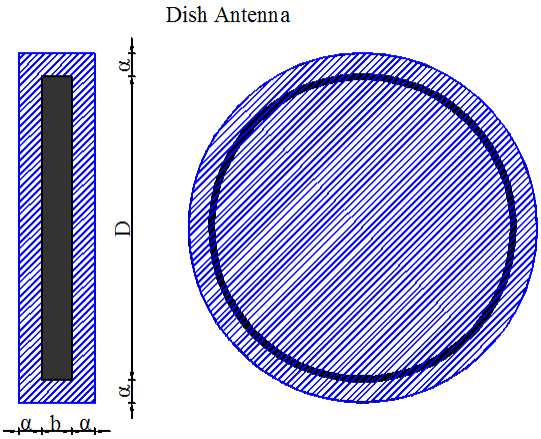

Ice Area:
$A_{ice} = (2\alpha + b)(D + 2a) - Db$ for side
$A_{ice} = \frac{\pi}{4}(D + 2a)^2$ for front view

Figure 2.6: Ice accretion model for each type of cross-section and the parabolic antennas.

2.3 Analyses

2.3.1 Pushover Analysis

As a first step, a pushover (nonlinear static) analysis was performed in order to specify the failure mechanisms of the tower. The lateral load profile considered in the pushover was following the pattern of the wind force as shown in Figure 2.4. Pushover analysis was conducted for no ice conditions and each of the icing scenarios. The results of the pushover analysis gave the top displacement along X axis at which the (first) failure occurs and the corresponding lateral load. It should be noted that the lateral loads are represented as a Load Factor (*LF*). LF is actually the factor that shows the relationship of the load at each step of pushover with the design load. In this case, *LF=1* corresponds to wind speed equal to 33 m/s, which is the design wind speed (V_b) of the tower.

2.3.2 Dynamic Analysis

The next step was the dynamic analysis of the tower. The main input for the nonlinear dynamic analysis was the time histories of the wind speed created in TurbSim software as discussed in Section 2.2.2.4. Thus, the wind speed value (i.e. the wind speed profile) was estimated for specific points at the heights of the horizontal diaphragms of the tower. The length of the time histories was 10 minutes (600 seconds).

The time histories of wind force along the height of the tower (i.e. the wind force profile) was done by processing the results of the time histories of wind speed and performing the necessary calculations by applying Eq. (2.1) along the two horizontal directions (X and Y). Thus, the wind force profile for the two horizontal directions was created. Those values constituted the inputs of the dynamic parameters for the OpenSees software where the dynamic analysis was performed.

A large number of dynamic analyses were performed for a range of values of (mean) wind speed and various wind angles, as it will be discussed in the corresponding sections. Finally, it should be noted that a damping equal to 1% was used based on results from relevant experiments [11] and experts' recommendation. The lower value of damping in comparison with steel buildings may be attributed to the fact a telecommunication tower is a bare steel structure without internal elements, such as walls, which contribute to the increase in damping.

2.4 Initial Tower

2.4.1 Member sections

As far as the legs are concerned, two types of angle sections were used. Specifically, the legs of the inclined section (height: 0-24m) were from L160.160.15, while the legs of the vertical section (height: 24-48m) from L120.120.12. For the main bracing diagonals, angle sections L70.70.7 were used throughout the whole height of the structure, while for the secondary diagonals L45.45.5 sections were used. The horizontal members of each diaphragm were composed from channel U100 sections. For the horizontal diagonal members angles L45.45.5 were used, except of the five levels of the working platforms where a channel U80 section was employed. The central horizontal member of each diaphragm was formed by a built-up section composed of 2 closely spaced channel U160 sections. Finally, the cross sections of the pyramid at the top of the tower (height: 48-51m) were L70.70.7.

2.4.2 Eigenvalue Analysis

The natural periods of the structure were determined by a modal analysis. Figure 2.7 presents the first three modes and the corresponding periods assuming no ice accretion on the tower. The first two modes have the same period due to structure's and loads symmetry, although they refer to different directions (X and Y). The third mode is torsional.

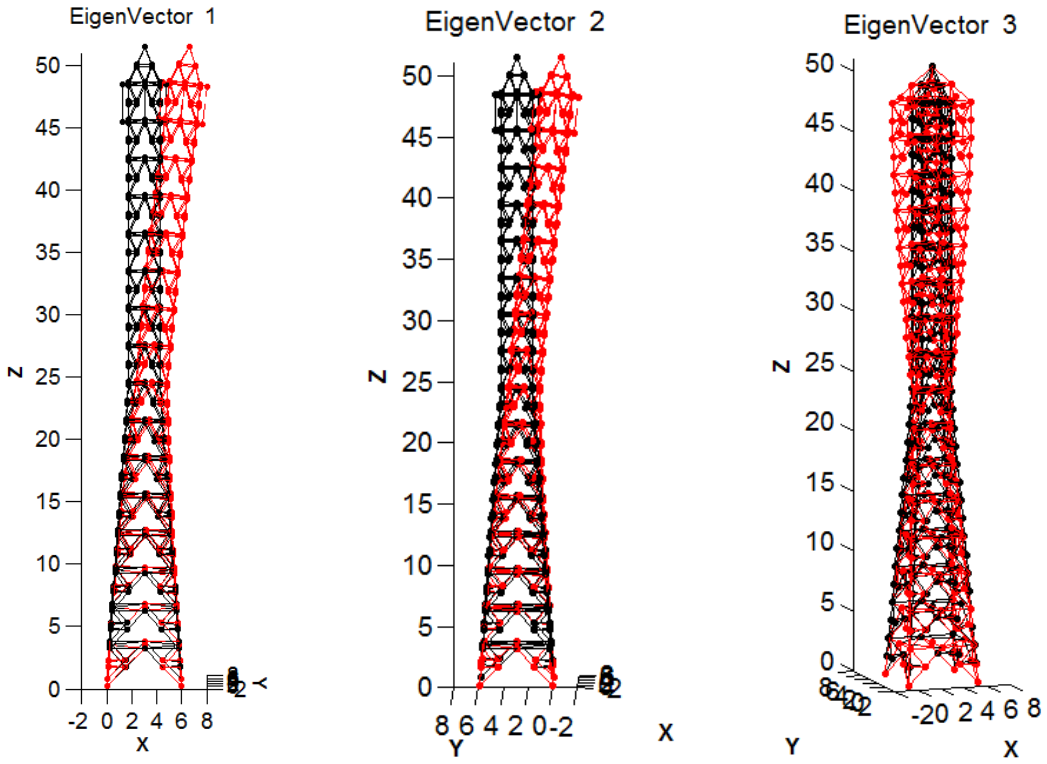

1st Mode — T_1=0.834 sec

2nd Mode — T_2=0.834 sec

3rd Mode — T_3=0.282 sec

Figure 2.7: First three modes and corresponding natural periods.

Modal analyses were also performed with various ice thickness scenarios. It is noteworthy, that as ice thickness increases the resulting natural periods are also increasing, probably due to the increase of the tower (and parabolic antennas) mass (Table 2.1).

Table 2.1: Natural periods of the first three modes for various icing scenarios

Ice Thickness (mm)	T_1 (sec)	T_2 (sec)	T_3 (sec)
1	0.834	0.834	0.281
5	0.900	0.900	0.302

2.4.3 Pushover Analysis

Following the results of the pushover analysis, it is evident that the first member failure occurs at the point of the tower where the inclination of the legs changes to vertical, a change which also coincides with the change in the legs' cross-section from L160.160.15 to L120.120.12 (Figure 2.8). The first element that fails could be either a leg or a main bracing member (marked with a red circle in the figure). As lateral loads increase, the failure cascades to other elements resulting finally in a total collapse.

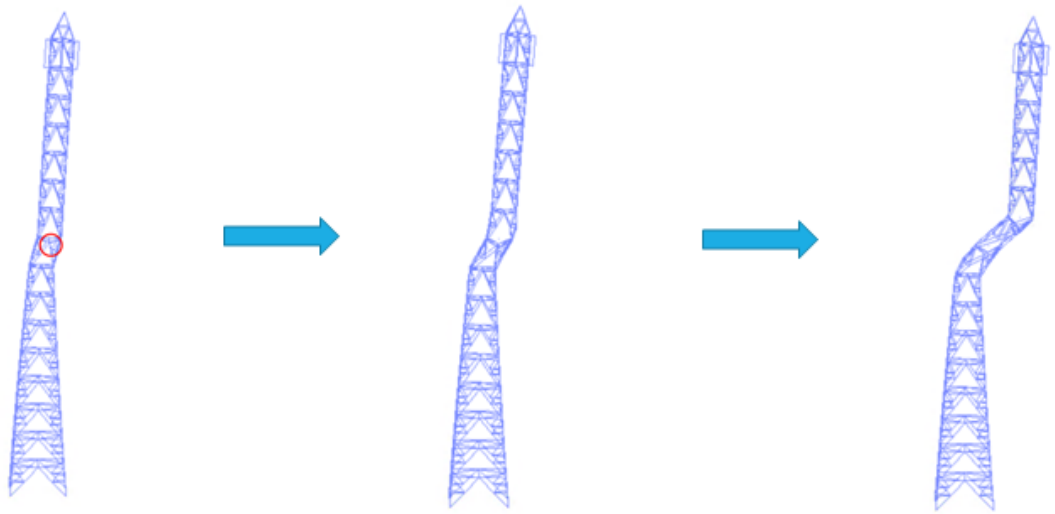

Figure 2.8: Failure mode as revealed by pushover analysis

Figure 2.9 presents the pushover curves for each of the icing scenarios considered. The horizontal axis depicts the displacement of the top of the tower along the lateral loads direction, while the vertical axis depicts the Load Factor (*LF*). The curves show that the maximum LF where the first failure occurs is for LF=3 (i.e. three times the design load). When ice is considered, the LF at first failure is lower. This should be attributed to the effect of ice both in mass and in projected areas which leads to increase in dead loads and wind forces. The corresponding displacement of the top (height 51 m) at the time of the first failure is approximately 0.41 m in all conditions.

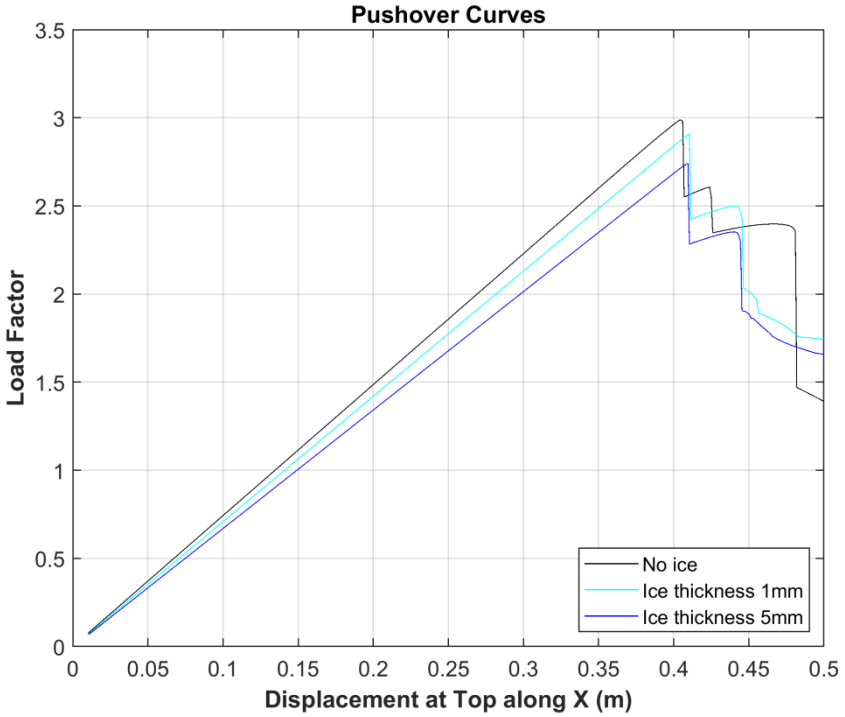

Figure 2.9: Pushover curves for various scenarios of ice thickness.

2.4.4 Dynamic Analysis

Figure 2.10 presents the typical results of the dynamic analyses regarding the top displacements along X. The time history of the graph at the left corresponds to a wind time history (input of analysis) with mean wind speed equal to 35 m/s at 10m and wind angle equal to 0 degrees assuming no ice conditions. On the other hand, the graph at the right corresponds to exactly the same time history of wind but assuming an ice layer of 5mm thickness accredited on the members and the parabolic antennas of the structure. As expected, the displacements of the top (especially the peaks of the time history) are slightly higher when ice is considered. This could be attributed to the larger acting wind forces due to ice accretion as discussed in a previous section. Finally, in both cases the displacement limit (orange line in the graphs) as calculated by pushover analysis (Figure 2.9) was not reached, and thus no failure was observed.

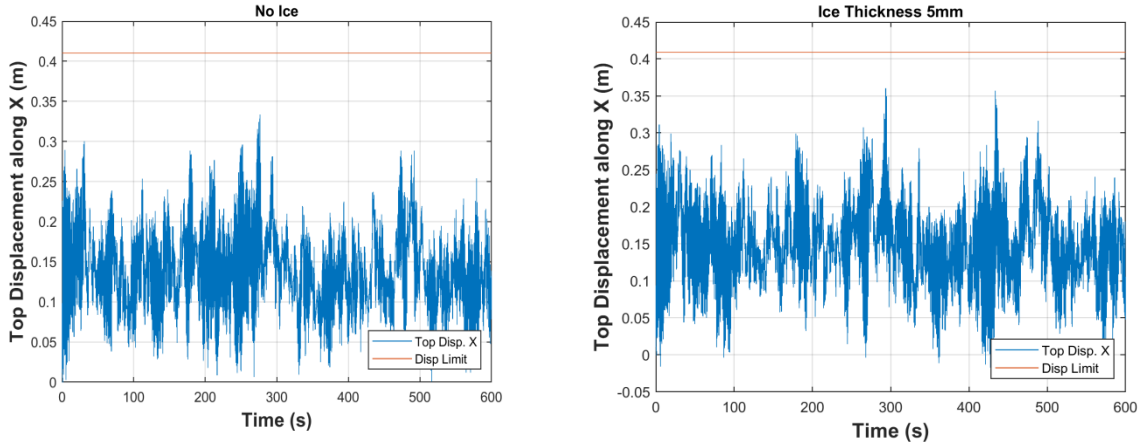

Figure 2.10: Typical time histories of Top Displacement along X (no failure case)

Figure 2.11 presents two similar time histories of top displacement to Figure 2.10. The wind time history (input of analysis) corresponds to mean wind speed of 40 m/s at 10m and wind angle of 0 degrees. In this case though, the displacement limit in the case of the ice scenario was exceeded and thus a failure was considered. So, it is observed that even for exactly the same time history of wind speed the outcome of the dynamic analysis (in terms of failure or not) could be different when ice is considered. This is actually evident if the results of pushover analysis (Figure 2.9) are considered, where the first failure occurs in a lower *LF* (i.e. wind speed) as the thickness of the ice layer increases.

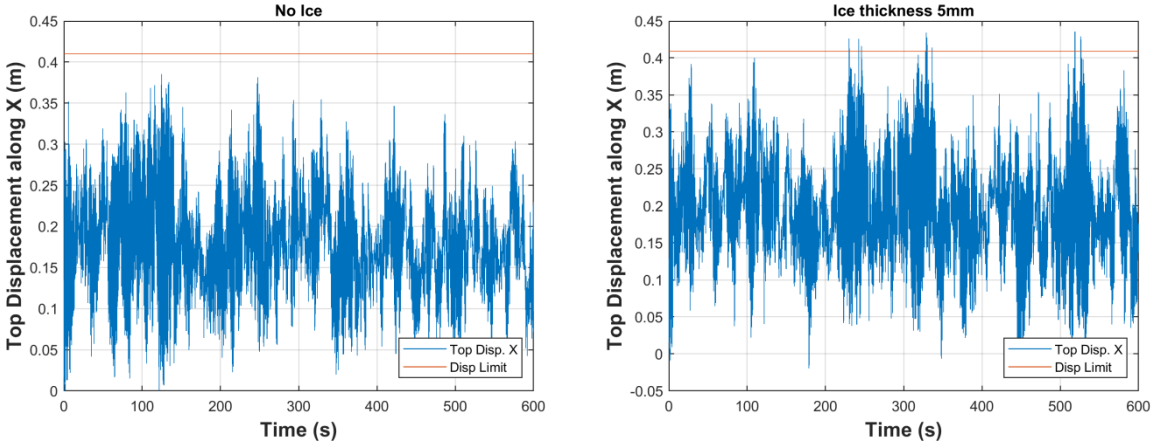

Figure 2.11: Typical time histories of Top Displacement along X (failure case)

Overall, the outcomes of each dynamic analysis performed were assessed following the context discussed above.

2.5 Corroded Tower

2.5.1 Corrosion assumptions

Corrosion is an important aging factor which contributes significantly to the degradation of the strength of steel members. Corrosion mainly reduces the cross-section parameters, such as size, area and moment of inertia. Thus, the overall strength of the structures weakens. Corrosion rate, i.e. the annual loss of cross-section reduction depends on various parameters such as the type of material (i.e. carbon steel, weathering steel, zinc, etc.) and the atmospheric environment of the structure. International standards [12]-[16] provide the classification of atmospheric environment and the corresponding typical values for corrosion rates.

According to ISO 9224 [14], the corrosion rate follows a bilinear pattern as shown in Figure 2.12. More specific, during the first 10 years of service life the average annual corrosion rate is constant and equal to r_{av}. After the first 10 years have passed the annual corrosion rate is usually lower and equal to r_{lin} until the end of the service life.

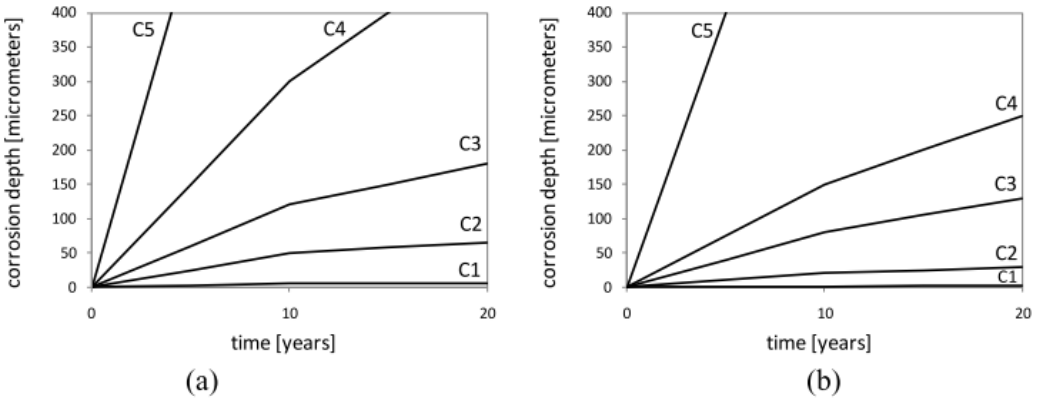

Figure 2.12: Thickness loss as a function of time (Source: [17]).

Herein, an atmospheric environment of category C4 that corresponds to high corrosity was assumed [18]. Furthermore, the thickness of zinc layer (galvanization) at the beginning of service was considered equal to 40 μm. Following the values provided by ISO 9224 [14], a r_{av} equal to 4μm/yr was considered for the zinc. Thus, the zinc layer was eliminated during the first 10 years of service. This value is considered for illustration purposes in the frame of the present analysis and does not represent actual conditions, where the corrosion protection systems are designed for a longer time. The remainder of cross-section was considered to be of carbon steel. For category C4 and carbon steel, the values of r_{av}=20μm/yr and r_{lin}=15μm/yr were adopted. The resulting carbon steel loss of thickness is presented in Figure 2.13. Eventually, the estimated loss of thickness for a service life of 60 years is equal to 0.8 mm.

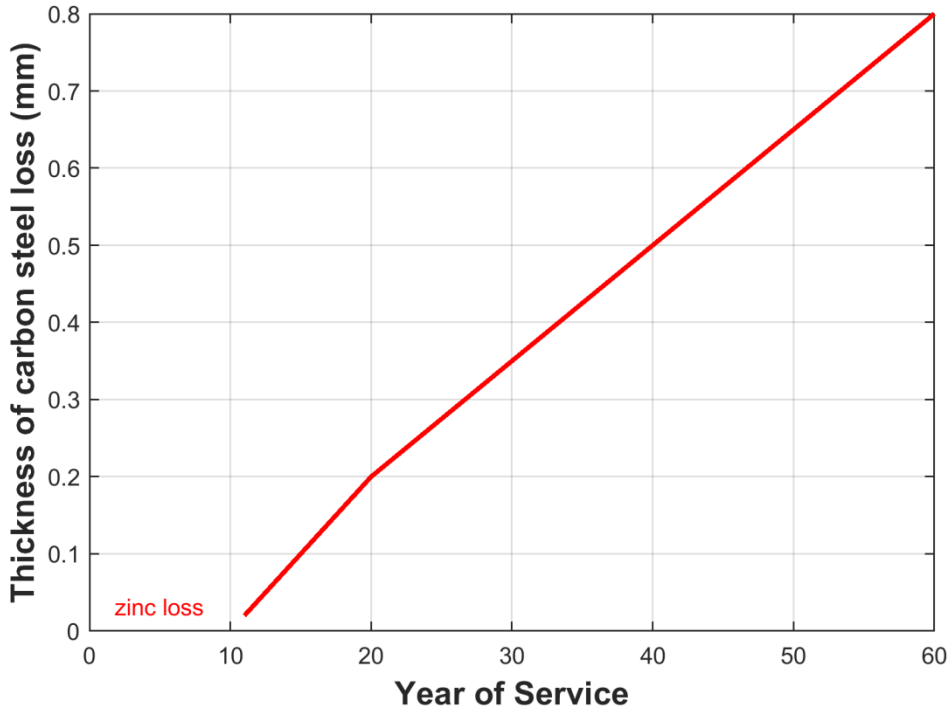

Figure 2.13: Loss of thickness during service life of the telecommunication tower.

2.5.2 Member sections

As mentioned in the previous section corrosion affects the size of a member's cross-section and its corresponding parameters. Following the estimation of corrosion as described above, the final dimensions of cross-section for the members of initial tower in the corroded state assuming 60 years of service are presented in Table 2.2

Table 2.2: Final dimensions of cross-sections of the telecommunication tower in the corroded state

Initial Cross-Section	Corroded State (in 60 yrs of service)				
	h (mm)	b (mm)	t (mm)	tf (mm)	tw (mm)
L160.160.15	158.4	158.4	13.4	N/A	N/A
L120.120.12	118.4	118.4	10.4	N/A	N/A
L70.70.7	68.4	68.4	5.4	N/A	N/A
L45.45.5	43.4	43.4	3.4	N/A	N/A
U80	78.4	43.4	N/A	6.4	4.4
U100	98.4	48.4	N/A	6.9	4.4
2U160	158.4	63.4	N/A	9.7	6.7

It is obvious that the smaller dimensions result in a reduction of the area of cross-section and the moments of inertia. This will reduce the strength of each member and will change the corresponding stress-strain curve (Figure 2.3).

Finally, it should be noted that in this work it was assumed that the projected areas of the members didn't change due to the effect of corrosion. Thus, the wind forces remain the same as in the case of the initial tower.

2.5.3 Eigenvalue Analysis

The natural periods of the corroded structure were determined by a modal analysis. They were slightly higher than those of the initial tower (Figure 2.7) as expected. This should be attributed to the lower moment of inertia and thus the lower stiffness of the corroded structure. Figure 2.14 presents the first three modes and the corresponding periods of the corroded tower assuming no ice accretion. The corresponding periods were estimated for the ice conditions and resulted in higher values.

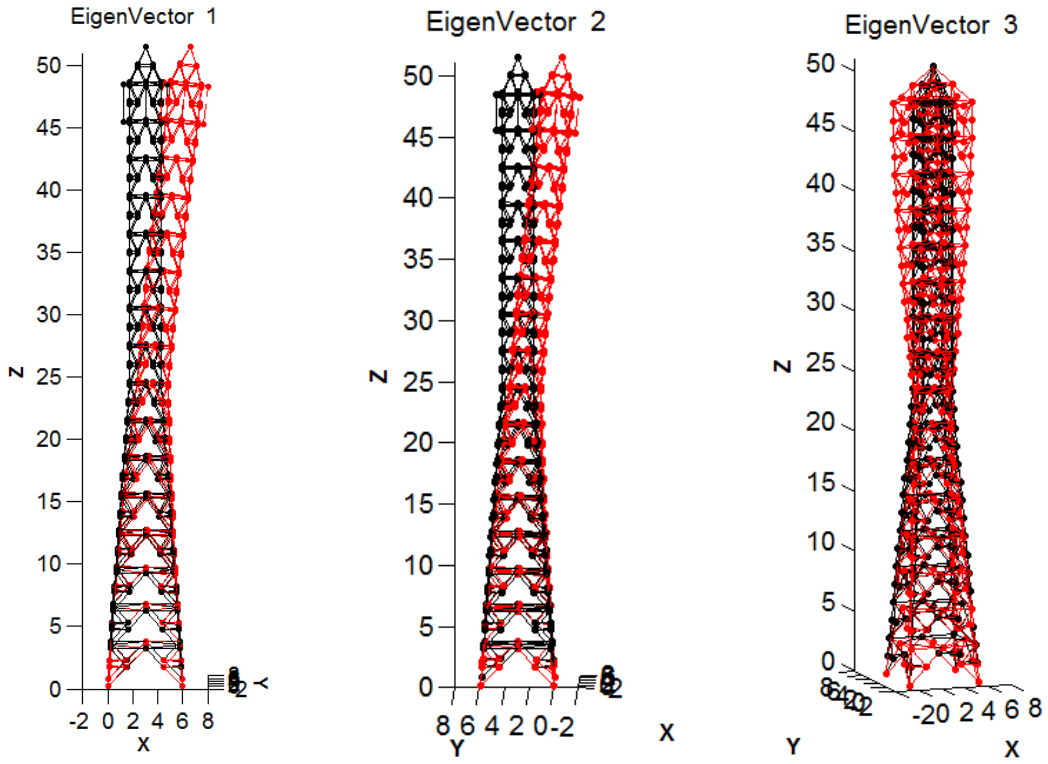

1st Mode	2nd Mode	3rd Mode
T_1=0.898 sec	T_2=0.898 sec	T_3=0.321 sec

Figure 2.14: First three modes and corresponding natural periods for the corroded tower.

2.5.4 Pushover Analysis

The pushover analysis of the corroded model (for no ice scenario) showed a similar pattern to the initial model. However, as shown on Figure 2.15, the maximum *LF* (where the failure occurs) was lower than the initial model and the top displacement at failure was also lower. The above findings are expected and should be attributed to lower strength of the corroded tower.

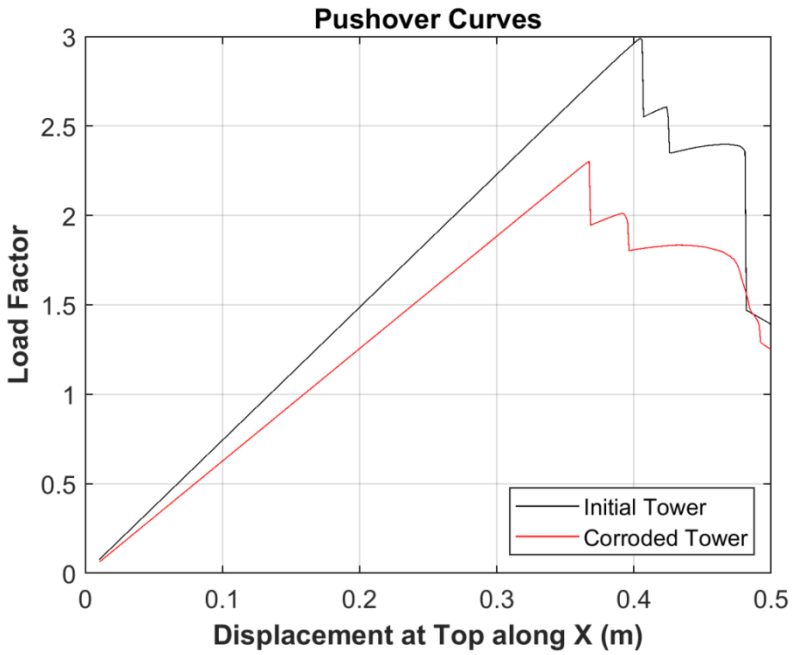

Figure 2.15: Pushover curves of the initial vs the corroded tower

2.5.5 Dynamic Analysis

Figure 2.16 presents typical of results of the dynamic analyses regarding the top displacements along X. The time history of the graph at the left corresponds to a wind time history (input of analysis) with mean wind speed equal to 35 m/s at 10m and wind angle equal to 0 degrees assuming no ice conditions. On the other hand, the graph at the right corresponds to exactly the same time history of wind but assuming an ice layer of 5mm thickness accredited on the members and the parabolic antennas of the structure. As expected, the displacements of the top (especially the peaks of the time history) are slightly higher when ice is considered. This could be attributed to the larger acting wind forces due to ice accretion as discussed in a previous section. In the case of the ice layer of 5mm the displacement limit (orange line in the graphs) as calculated by pushover analysis (Figure 2.9) was exceeded, and thus that case was considered as a failure of the tower. On the other hand, no failure was observed when no ice conditions scenario was assumed (displacement limit not exceeded). Finally, it is observed that the same mean wind speed results in larger displacements of the top of the tower in the corroded model that in the case of the initial model (Figure 2.10).

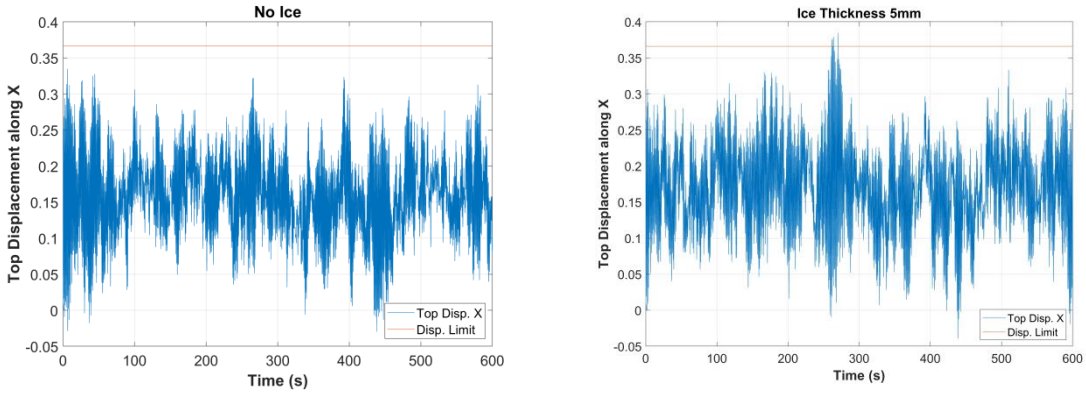

Figure 2.16: Typical time histories of Top Displacement along X of the corroded tower

2.6 Strengthened Hybrid Member Tower

2.6.1 Strengthening methodology

A new innovative strengthening method was applied on the existing (corroded) tower. FRP plates were attached on the existing angle members, instead of replacing brace members with new ones or adding extra members to make built-up members. In this way, it was possible to increase the buckling resistance of a limited number of selected members, in certain parts of the tower, without any increase in tower's total weight or wind reference area. Table 2.3 includes the properties of the FRP material. Since the purpose of this investigation is not the design but a performance assessment for the lattice tower, the mean values were used in the analysis, instead of the 5%-fractile values.

Table 2.3: FRP material properties (mean values)

FRP material properties	E (GPa)	fu (MPa)
	170	3100

FRP strengthening was applied only to the main tower's members, legs or primary braces. Depending on the angle's size, several types of FRP plates can be used. Table 2.4 includes all the appropriate types of FRP plates with their properties, that can be applied on existing tower's members.

Table 2.4: FRP plates used for strengthening tower's members

Type of member	Existing angle section	Appropriate FRP plate
Leg (height 0-24m)	L160.15	S 1512 (b=150mm, t=1.2)
Leg (height 24-48m)	L120.12	S 1012 (b=100mm, t=1.2)
Brace	L70.7	S 512 (b=50mm, t=1.2)

It was assumed that FRP plates were placed only externally to both legs of the existing angle section, as shown in Figure 2.17, to make the hybrid member. Calculation of tension and buckling resistance of strengthened-hybrid members is analytically described in Deliverable 4.4 (Design guide) [19]. Regarding the angle steel section, cross-section properties were considered for members in the corroded state (see section 2.5.2). In numerical simulations, the hybrid cross-section was transformed into an equivalent steel section with the mechanical properties of the hybrid section.

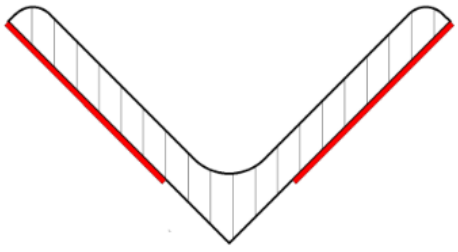

Figure 2.17: Hybrid member composed of existing angle section and FRP plates placed externally

2.6.2 Strengthened Members

Strengthening with FRP plates was selected for the members of the most vulnerable part ("sensitive area") of the corroded tower. The "sensitive area" was actually the part of the tower, where the inclination of the legs changes to vertical, as revealed by the failure mode via pushover analysis

(Figure 2.18). Legs or bracing members between heights from 24 to 33m were selected for strengthening (indicated in red in Figure 2.18).

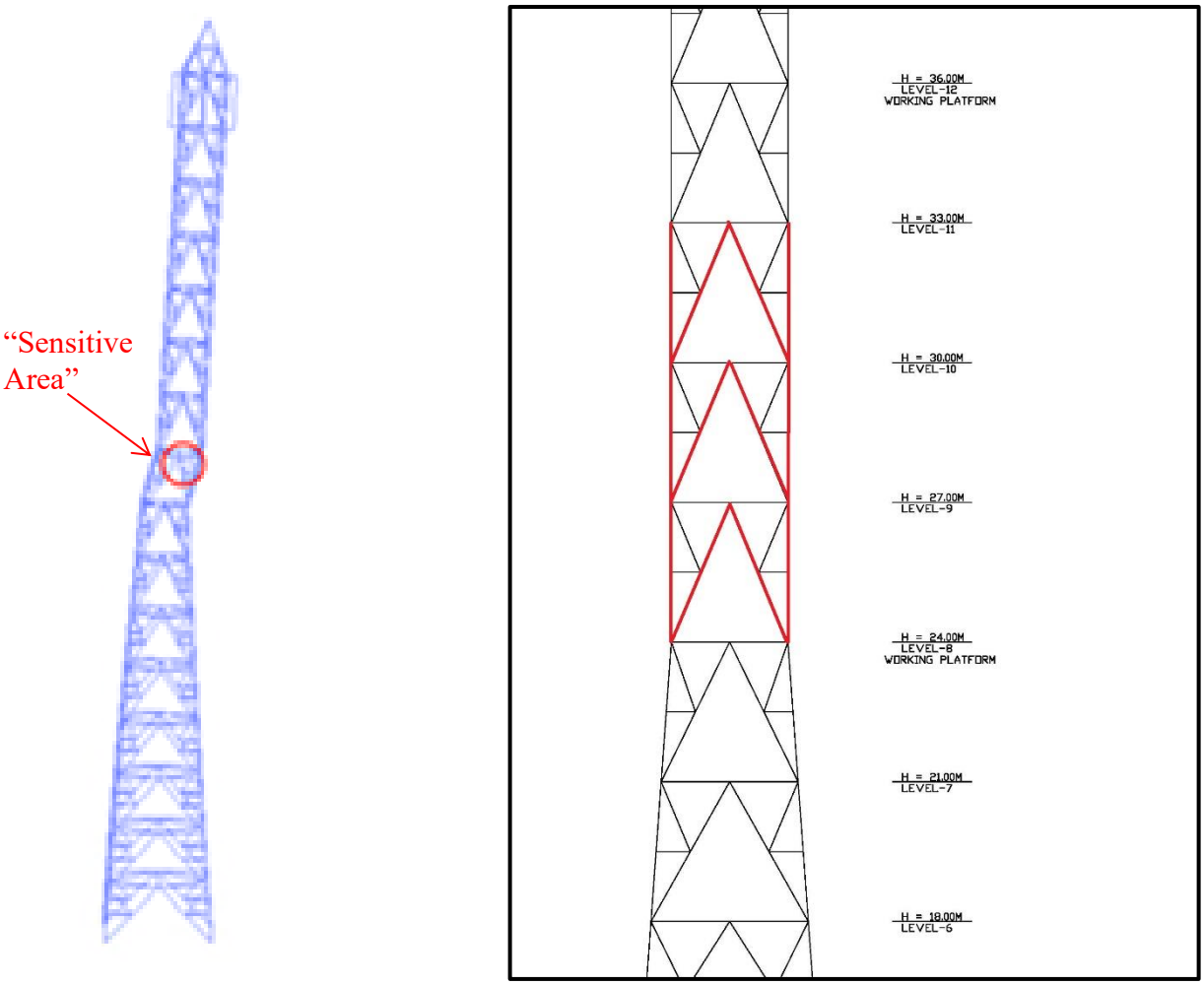

Figure 2.18: Part of the corroded tower strengthened with FRP plates ("Sensitive Area")

Three scenarios of strengthening were considered before the dynamic analysis of the tower. The first scenario included strengthening both all legs and bracing members of the sensitive area (heights 24-33m). In the second scenario only the legs of the sensitive area were strengthened, while in third only the main bracing members were selected for strengthening.

2.6.3 Eigenvalue Analysis

Figure 2.19 presents the first three modes and the corresponding periods of the strengthened hybrid tower assuming no ice accretion. The values of the first two eigenperiods are higher than those of the initial and corroded towers. This could be attributed to the lower moment of inertia and thus the lower stiffness of the strengthened members.

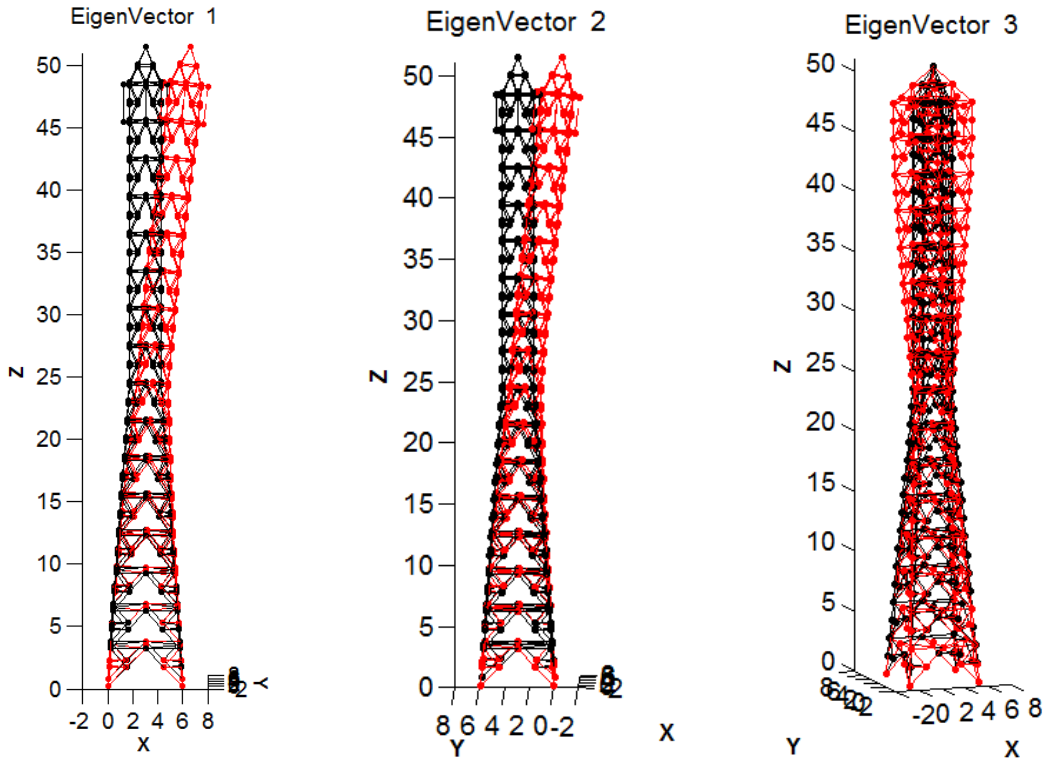

1st Mode
T_1=0.904 sec

2nd Mode
T_2=0.904 sec

3rd Mode
T_3=0.315 sec

Figure 2.19: First three modes and corresponding natural periods for the strengthened with FRPs tower.

2.6.4 Pushover Analysis

Figure 2.20 shows the pushover curves for each of the three strengthening scenarios. Furthermore, the corresponding pushover curves of the initial tower and the corroded model (Figure 2.15) are presented for comparison.

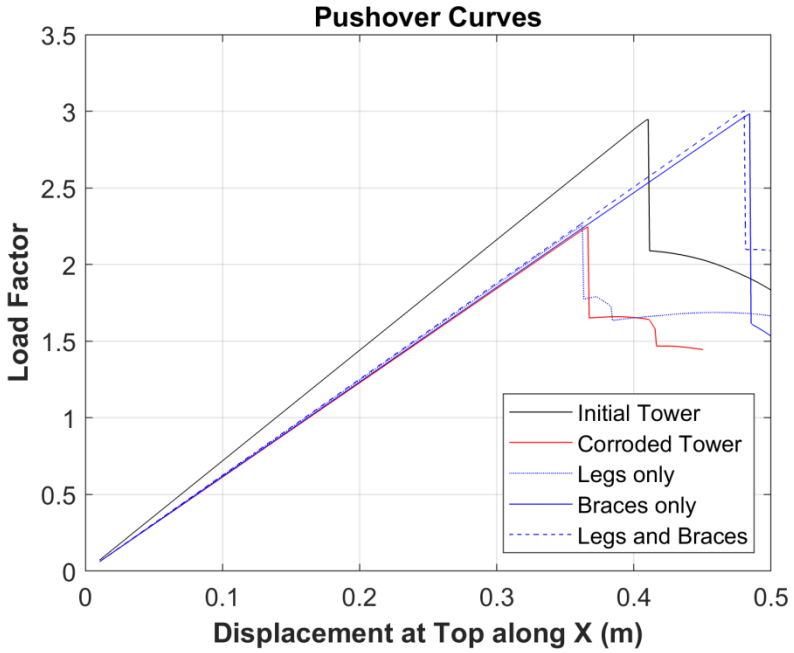

Figure 2.20: Pushover curves of the three scenarios of strengthening with FRPs

Pushover curves show that strengthening legs only provides the smallest benefit and does not change the strength of the corroded tower much, probably because failure occurs firstly in bracing members. Indeed, strengthening legs only results in the same *LF* when the first failure occurs with the corroded model (*LF=2.30*). On the other hand, when only the bracing members were strengthened, the *LF* (about 2.98) when the first failure occurs is larger than that of the corroded model and close to the initial model (*LF=2.94*). Finally, in the third scenario, when both legs and bracings were strengthened, the resulting *LF* at first failure was the highest and equal to 3.00. Thus, only the scenarios which include strengthening of bracing members provide a considerable increase in the strength of the corroded tower which reaches the level of strength of the initial tower. Moreover, strengthening both legs and bracing members seems to have the same effect with strengthening the bracing members only.

Considering the above, strengthening only the bracing members seems to be the preferred solution in terms of a cost-benefit perspective (less FRP plates and worktime needed). Thus, the corresponding strengthening scenario was selected for further analysis as the strengthened with hybrid members case.

2.6.5 Dynamic Analysis

Figure 2.21 presents typical results of the dynamic analyses regarding the top displacements along X of the strengthened with FRPs tower. The time history of the graph at the left corresponds to a wind time history (input of analysis) with mean wind speed equal to 35 m/s at 10m and wind angle equal to 0 degrees assuming no ice conditions. On the other hand, the graph at the right corresponds to exactly the same time history of wind but assuming an ice layer of 5mm thickness accredited on the members and the parabolic antennas of the structure. As expected, the displacements of the top (especially the peaks of the time history) are slightly higher when ice is considered. This could be attributed to the larger acting wind forces due to ice accretion as discussed in a previous section. However, in both scenarios (no ice and ice thickness of 5mm) the displacement limit is not reached and thus no failure was observed. This finding also reveals the effect of strengthened members on the corroded tower. Since, as shown in Figure 2.16, the same wind speed caused a failure of the corroded tower when an ice layer of 5mm was considered.

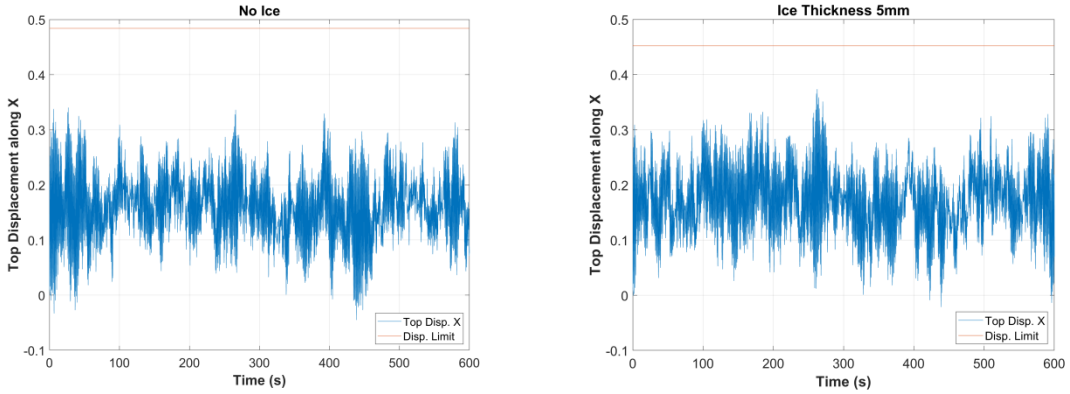

Figure 2.21: Typical time histories of Top Displacement along X of the strengthened with FRP tower

2.7 High Strength Steel member Tower

2.7.1 Redesign with High Strength Steel

A redesigned version of the initial model with High Strength Steel (HSS) was the last case study of the telecommunication tower in this task. The HSS tower had the same geometry with the initial one. In terms of steel grades, two different grades were assumed. In specific, S460 was used for the legs and the main bracing diagonal members and S355 for the rest of the members. It should be noted that, as in all cases of the towers considered herein, the actual values for the yielding and ultimate stresses were used as proposed by [2]. For the S460 steel grade, the actual yield stress was considered equal to 495.26 MPa and the ultimate stress equal to 620.98 MPa. The corresponding values for the S355 grade were 414.09 MPa and 546.16 MPa, respectively.

As far as the member sections are concerned, the legs of the inclined (bottom) part of the tower were from L140.140.15, while the legs of the vertical part were from L110.110.12. The main bracing diagonal members were from L60.60.6, with the exception of the "sensitive area" (height: 24 - 33m) where L70.70.7 was used. The rest of the tower members were designed with the same sections as in the initial tower, but with higher steel grade (S355 instead of S235). Table 2.5 presents all the sections used in the initial and HSS model for the sake of comparison.

Table 2.5: Member sections in Initial and HSS Towers

Member Type	Initial Tower		HSS Tower	
	Cross-Section	Steel Grade	Cross-Section	Steel Grade
Leg (inclined part)	L160.160.15	S235	L140.140.15	S460
Leg (vertical part)	L120.120.12	S235	L110.110.12	S460
Vertical Diagonal/Main Bracing Diagonal	L70.70.7	S235	L60.60.6*	S460
Secondary Bracing	L45.45.5	S235	L45.45.5	S355
Horizontal Diagonal**	U80	S235	U80	S355
Horizontal	U100	S235	U100	S355
Horizontal Member for ladder support	2U160	S235	2U160	S355

* L70.70.7 was used for Vertical Diagonals in the "sensitive area"

** U80 was used for Horizontal Diagonals on the working platforms and L45.5 elsewhere

2.7.2 Eigenvalue Analysis

Figure 2.22 presents the first three modes and the corresponding periods of the corroded tower assuming no ice accretion. The values of the first two eigenperiods are larger than the corresponding values of the initial model, but lower than those of the corroded and the FRP strengthened models.

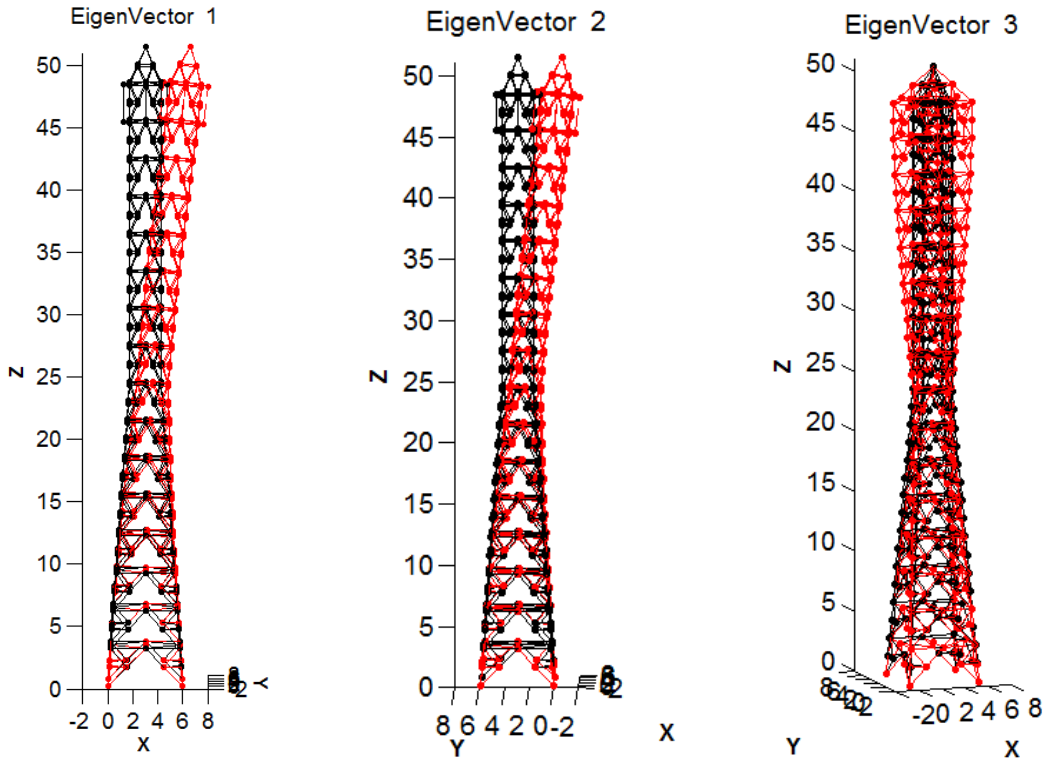

1st Mode
T_1=0.887 sec

2nd Mode
T_2=0.887 sec

3rd Mode
T_3=0.303 sec

Figure 2.22: First three modes and corresponding natural periods for the HSS tower.

2.7.3 Pushover Analysis

Figure 2.23 shows the pushover curve (green line) for the HSS tower. Furthermore, the corresponding pushover curves of the initial, the corroded and the strengthened hybrid member towers are presented for the sake of comparison.

According to the results of the pushover analysis, the highest *LF* corresponds to the case of the HSS tower. In that case, the *LF* when the first failure occurs is equal to 3.78. In addition, the top displacement at the time of first failure is much larger than any of the other models and equal 0.553m.

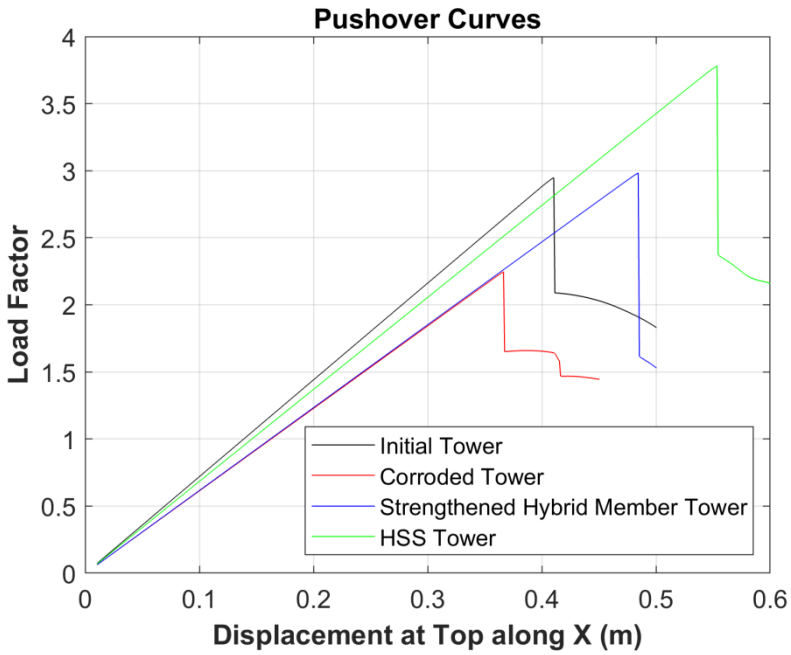

Figure 2.23: Pushover curves of the four versions of telecommunication towers

2.7.4 Dynamic Analysis

Figure 2.24 presents typical results of the dynamic analyses regarding the top displacements along X of the HSS tower. The time history of the graph at the left corresponds to a wind time history (input of analysis) with mean wind speed equal to 35 m/s at 10m and wind angle equal to 0 degrees assuming no ice conditions. It is observed that the top displacements along X are lower than the displacement limits of failure for both icing scenarios.

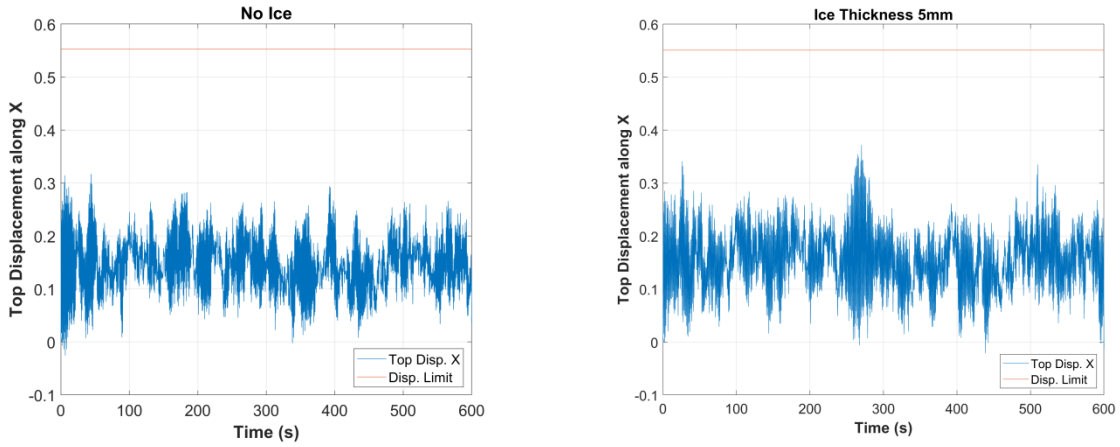

Figure 2.24: Typical time histories of Top Displacement along X of the HSS tower

3 Suspension Power Transmission Tower

3.1 Structural description and modelling

3.1.1 Geometry

A standard Danube tower that is widely used in Central Europe is considered in the present case study. It has been designed according to the German National Annex of EN 50341-1:2012. The tower has a standard height of 50m and two cross-arms with different lengths. The lower cross-arm's length is 31m while the upper's is 22m. The main body of the tower has square cross-section (6.84m by 6.84m at the base) whose dimensions reduce with height. Figure 3.1 shows the tower configuration separated in a number of segments along its height. The tower members are made by hot-dip galvanised equal-leg angle profiles of various sizes.

The tower is assumed to be a suspension (support) tower carrying two 380 kV circuits each of them consisting of three phases. Each phase is made of a bundle of four conductors supported by a suspension insulator hanging vertically. Furthermore, a single earth-wire is installed on the top of the tower for lighting protection. The type 264-AL1/34-ST1A was selected for conductors, while 94-AL1/15-ST1A is employed for the earth-wire. Finally, the Quadril*Sil insulator S025185S201 made of silicone rubber having a length of 5m and a weight of 87N (i.e. 9 kg) was selected. A detailed description of the tower's geometry and additional specifications are provided in [1],[20].

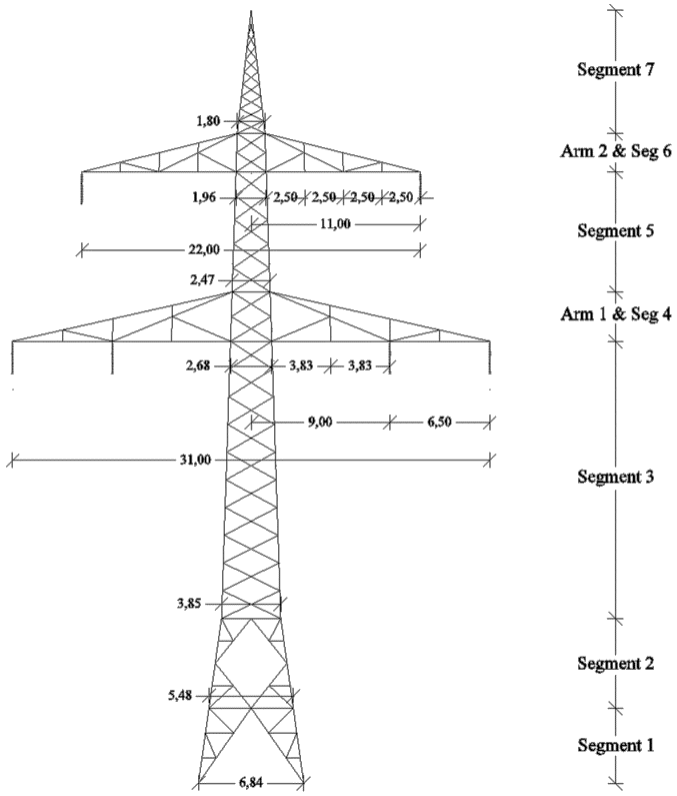

Figure 3.1: Danube tower configuration (Source:[20])

3.1.2 Material

The structural steel grade is S355J2 for all members of the tower. At this point it should be noted that since the goal is not the design but a performance assessment for a power transmission tower, the expected values of steel strength were employed in the model, instead of the nominal ones.

Specifically, for steel grade S355J2, the (mean) yield strength f_y is set equal to 414.09 MPa and the (mean) tensile strength f_u is equal to 546.16 MPa [2]. The material stress-strain curve that was assumed in the analysis is presented in Figure 3.2. The modulus of elasticity of steel is taken as E=210GPa. Fiber sections were employed together with beam-column and truss elements to model the tower. To assign stress-strain relationships to each steel fiber, the general form of Figure 3.2 was employed as stress-strain curve in compression and tension, using the buckling reduction factor χ, as calculated for each structural member according to EN 1993-3-1 [3], to account for compression buckling.

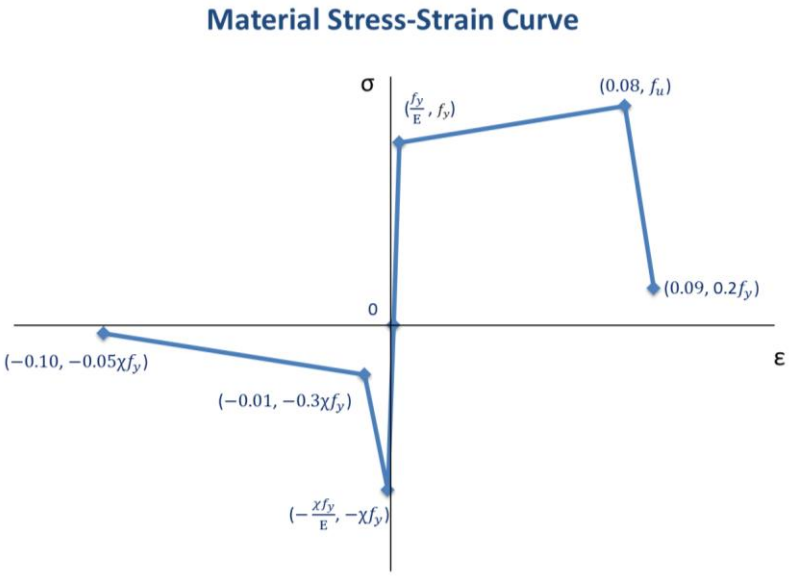

Figure 3.2: General form of a member stress-strain curve

3.2 Loads

3.2.1 Gravity Loads

The total weight of all tower members was calculated after multiplying the length of each member by the corresponding unit weight of the member's angle profile. For each of the six insulators considered in the model the weight was estimated to be 87N, resulting in a total weight of 522N (i.e. 45 kg).

3.2.2 Wind Load at the tower

The wind force acting on the transmission tower is calculated following a similar process as described in Section 2.2.2.1 for the telecommunication antenna. For the calculations, each of the segments of the tower (Figure 3.1) was divided into sub-segments of approximately 1.5 m height. Then, the solidity ratio φ of each sub-segment was calculated and the resulting wind force was estimated using Eq. (2.2) and considering the corresponding wind speed for each sub-segment based on its height. Finally, the wind force was assigned to the corner nodes of each sub-segment.

3.2.2.1 Wind Speed Profile and Wind Field Simulation

A similar process as described in Section 2.2.2.3 was applied for the estimation of the wind speed values (i.e. wind profile) along the height of the tower using the same assumptions as in the case of the telecommunication antenna.

The TurbSim software was also used for the wind field simulation. However, in this case the simulated wind field had a width equal to a span length in order to simulate the wind speeds along the conductors' length for the corresponding calculations as they will be described in Section 3.2.4.

3.2.3 Ice Loads on tower

The ice loads were estimated by assuming ice layer of uniform thickness accumulated on the exposed surfaces of the tower members following the process described in Section 2.2.3. Finally, a number of scenarios of various ice thicknesses were applied as in the case of the telecommunication antenna.

3.2.4 Conductor and Insulator Loads

When a conductor is suspended between two points (e.g. two insulators of adjacent towers) it forms a catenary curve [21]-[22]. The mathematical expression of this curve is given by the following equation:

$$y = C\left(\cosh\frac{x}{C} - 1\right) \qquad \text{Eq. 3.1}$$

where:

$$C = \frac{H}{W} \qquad \text{Eq. 3.2}$$

H is the horizontal tension force and W the weight of the conductor.

The total force acting at the end of the conductor, T_{supp}, is calculated by combining the horizontal and vertical reaction, Tx, Ty (Figure 3.3a) as follows:

$$T_x = H \qquad \text{Eq. 3.3}$$

$$T_y = \frac{wL}{2}$$

$$T_{supp} = \sqrt{{T_x}^2 + {T_y}^2}$$

Both wind and ice have a significant effect on the conductor's sag and tension. Assuming that a layer of ice thickness t (Figure 3.3b) has been formed around the conductor, then the additional weight W_{ice} due to ice is calculated as:

$$W_{ice} = \rho_{ice} V_{ice} = \rho_{ice}\pi t(D + t) \qquad \text{Eq. 3.4}$$

where ρ_{ice} is the ice density and D the diameter of the conductor.

If at the same time a wind of speed u over the above conductor is applied, then the additional force W_{wind} per unit length due to wind is:

$$W_{wind} = q(D + 2t) \qquad \text{Eq. 3.5}$$

where: q is the dynamic pressure of the wind.

Thus, the total force per unit length due to conductor's own weight, wind and ice is equal to:

$$W_{total} = \sqrt{(W + W_{ice})^2 + {W_{wind}}^2} \qquad \text{Eq. 3.6}$$

When the conductor is installed (i.e. strung) it obtains an initial horizontal tension H_1 which is mainly affected by the temperature during installation. The final tension H_2 in the conductor including the effect of ice and wind is calculated by solving the following Equation, assuming a parabolic sag-line of the conductor:

$$H_2{}^3 + H_2{}^2 \left(\frac{(W_1 S)^2 AE}{24 H_1{}^2} - H_2 + (t_2 - t_1) aAE\right) - \frac{(W_2 S)^2 AE}{24} = 0 \qquad \text{Eq. 3.7}$$

W_1 is the unit weight of the conductor at initial temperature, W_2 is the unit weight of the conductor at final temperature (i.e. to be taken as the total unit force W_{total} to also account for wind and ice), t_1 and t_2 are the initial and final temperature (°C) respectively, S is the span length (m), a is the coefficient of linear thermal expansion, E is the conductor's modulus of elasticity (Pa), and A is the conductor's cross-sectional area (m^2).

Herein, the span length was assumed equal to 350m, the initial temperature 10°C and the final temperature 10°C for the no ice conditions and 0°C for the icing conditions. The tension and the sag of the conductors and the earth-wire were estimated for various values of wind speeds and ice thicknesses. The wind speeds were simulated every 50m along the length of the span (width of wind field) and their average value was used in the calculations. Finally, based on the above equations, the loads due to conductors and earth-wire were estimated and applied in the model of the tower. It should be noted that the aforementioned Equations are valid for one bundle. In the case of the four-bundled conductors the results are multiplied by four.

The wind force at an insulator F_{ins} is simply estimated by applying the following equation:

$$F_{ins} = qC_D A_{ref} = qC_D(D_{ins} + t) \qquad \text{Eq. 3.8}$$

where q is the dynamic pressure of the wind, D_{ins} is the diameter (m) of the insulator, t is the ice thickness (if applicable) and C_D the drag coefficient assumed here equal to 1.20.

a)

b)

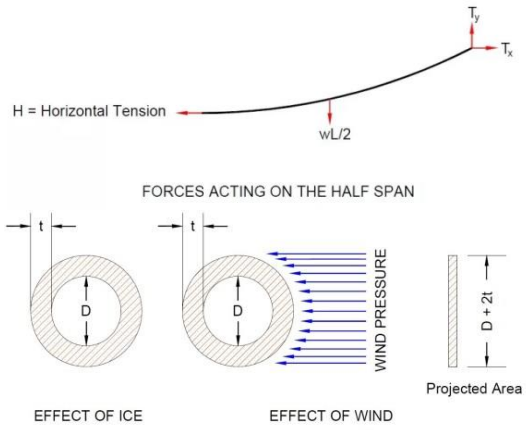

Figure 3.3: a) Forces acting at half span of a conductor, b) Effects of ice and wind (Source [22])

3.3 Initial Tower

3.3.1 Member sections

All members of the transmission tower were composed from equal leg angles of various sizes listed in Table 3.1. Furthermore, the members were grouped in various groups according to their size and location in the tower as shown in Figure 3.4. A more detailed description of the tower members is provided by [1].

Table 3.1: Angle profiles used for the members of the suspension tower

Group	Angle Type	Angle Size	Steel grade
Bottom-legs	SAE	AM 150x150x13-/+	S355J2
Segment 2	SAE	AM 140x140x15	S355J2
Segment 3	SAE	AM 120x120x16	S355J2
Segment 4	SAE	AM 80x80x10-	S355J2
Segment 5	SAE	AM 80x80x6	S355J2
Segment 6	SAE	AM 75x75x4	S355J2
Segment 7	SAE	AM 45x45x3	S355J2
Diagonal 1	SAE	AM 75x75x4	S355J2
Diagonal 2	SAE	AM 75x75x4	S355J2
Diagonal 3	SAE	AM 90x90x5	S355J2
Diagonal 4	SAE	AM 90x90x6	S355J2
Diagonal 5	SAE	AM 60x60x4	S355J2
Diagonal 6	SAE	AM 45x45x4	S355J2
Cross 1-bottom	SAE	AM 150x150x12-/+	S355J2
Cross 1-top	SAE	AM 120x120x7	S355J2
Cross 1-base	SAE	AM 130x130x8	S355J2
Horizontal 1	SAE	AM 80x80x5	S355J2
Horizontal 2	SAE	AM 90x90x5	S355J2
Horizontal 3	SAE	AM 100x100x7	S355J2
Horizontal 4	SAE	AM 76x76x4.8	S355J2
Horizontal 5	SAE	AM 75x75x6-	S355J2
Horizontal 6	SAE	AM 65x65x4	S355J2
Horizontal 1 base	SAE	AM 80x80x5	S355J2
Horizontal 2 base	SAE	AM 80x80x5	S355J2
Horizontal 3 base	SAE	AM 76x76x4.8	S355J2
Horizontal 4 base	SAE	AM 60x60x4	S355J2
Cross - Horizontal	SAE	AM 45x45x3	S355J2
Cross 2-bottom	SAE	AM 120x120x7	S355J2
Cross 2-top	SAE	AM 75x75x5	S355J2
Cross 2-base	SAE	AM 90x90x5	S355J2
Redundant 1	SAE	AM 90x90x5	S355J2
Redundant 2	SAE	AM 60x60x4	S355J2
Redundant 3	SAE	AM 90x90x5	S355J3

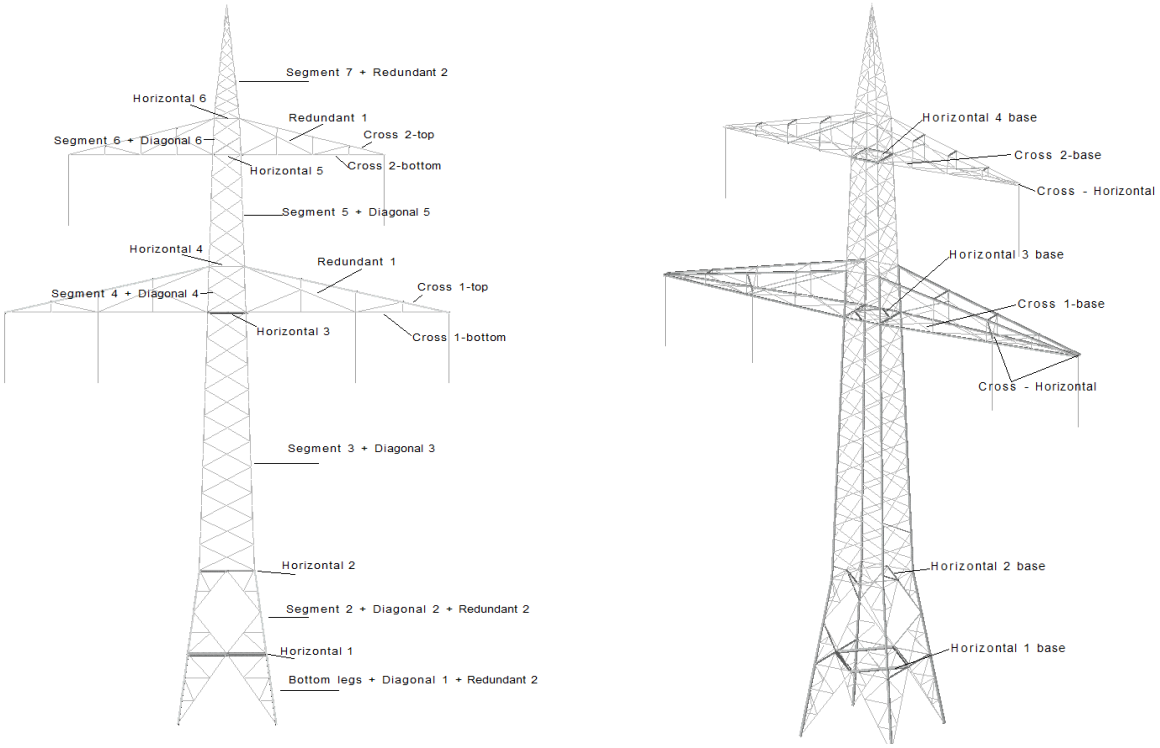

Figure 3.4: Annotations of the various group of members and their position on the tower (Source: [1])

3.3.2 Eigenvalue Analysis

The natural frequencies of the structure were determined by modal analysis. The first two modes are longitudinal (directions X and Y) and the third mode is torsional (Figure 3.5). Modal analyses were also performed for each of the icing scenarios. Table 3.2 presents the periods of the first three modes for various scenarios considered herein. The results show, as expected, that as the thickness of the ice layer increases, the corresponding periods increase. Certainly, this should be attributed to the increase of the tower mass.

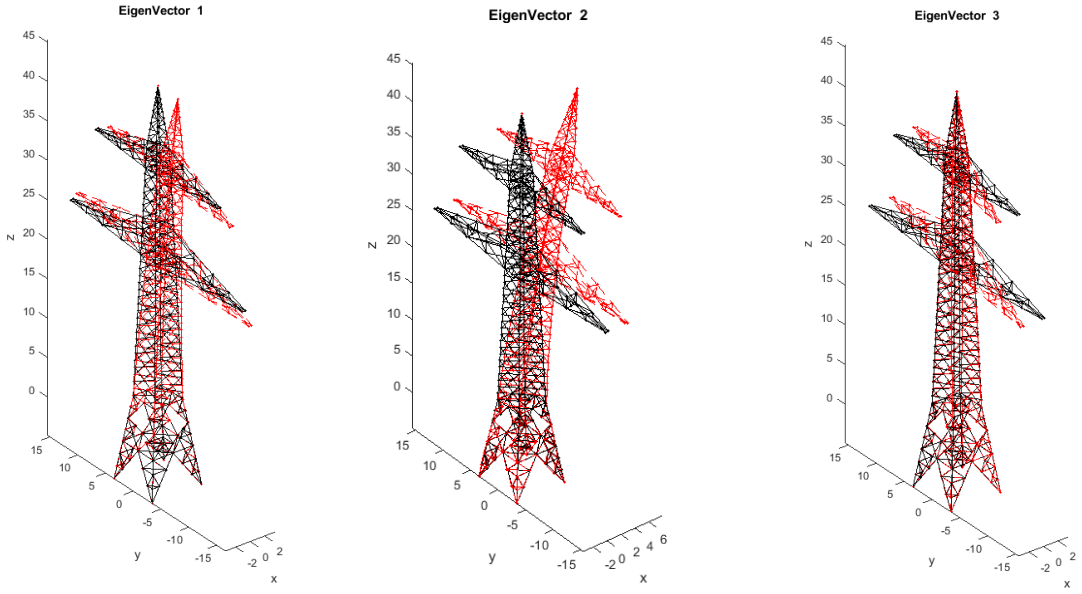

1st Mode — *T_1=0.510 sec*

2nd Mode — *T_2=0.503 sec*

3rd Mode — *T_3=0.434 sec*

Figure 3.5: First three modes and corresponding natural periods

Table 3.2: Natural periods of the first three modes for various icing scenarios

Ice Thickness (mm)	T_1 (sec)	T_2 (sec)	T_3 (sec)
1	0.520	0.513	0.440
10	0.605	0.597	0.495
15	0.656	0.646	0.526

3.3.3 Pushover Analysis

As a first step before the nonlinear dynamic analysis, a pushover (nonlinear static) analysis was performed in order to understand the failure mechanisms of the tower. A lateral load profile transverse to the direction of the line is considered following the power-law pattern of the wind speed. Pushover analysis was conducted for various scenarios of icing. In all cases, the top pyramidal segment 7 of the tower (Figure 3.1), supporting the earth-wire, fails first, even at low wind speeds. This was subsequently strengthened and the dominant failure became the buckling of the worst-loaded composite leg, which becomes a runaway failure of the entire compression side, as shown in Figure 3.6. The first failure occurs at segment 2 of the tower where the members form a

rhomboid shape. This failure is consistent with experience from transmission tower failures in past severe storms [23] and tests [24].

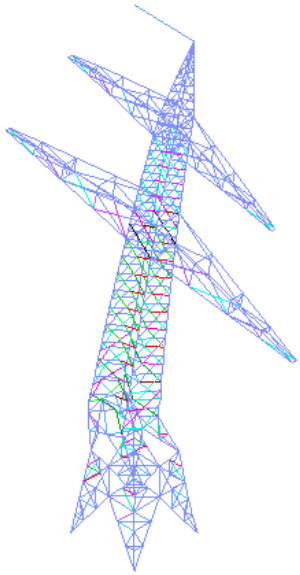

Figure 3.6: Failure mode of suspension tower as revealed by pushover analysis

Figure 3.7 presents the pushover curves for various icing scenarios. The horizontal axis depicts the displacement of the top of the tower along the lateral load direction (transverse to the transmission line), while the vertical axis depicts the Load Factor (LF). A Load Factor equal to 1 (*LF=1*) corresponds to the load caused by a wind speed at a height of 10m equal to the basic wind speed used in the design, i.e. 25 m/s. For example, at the no ice scenario, the failure occurs when the top displacement in the direction transverse to the transmission line reaches 0.556m. At this point the LF is about 2.18 which means that the lateral loads at the time of the first member failure is 2.18 times larger than the lateral loads that correspond to a reference wind speed of 25 m/s at 10m. Figure 3.7 also shows that as the thickness of the ice layer on the structure and conductors increases, the first failure occurs in lower LF values and lower top displacements.

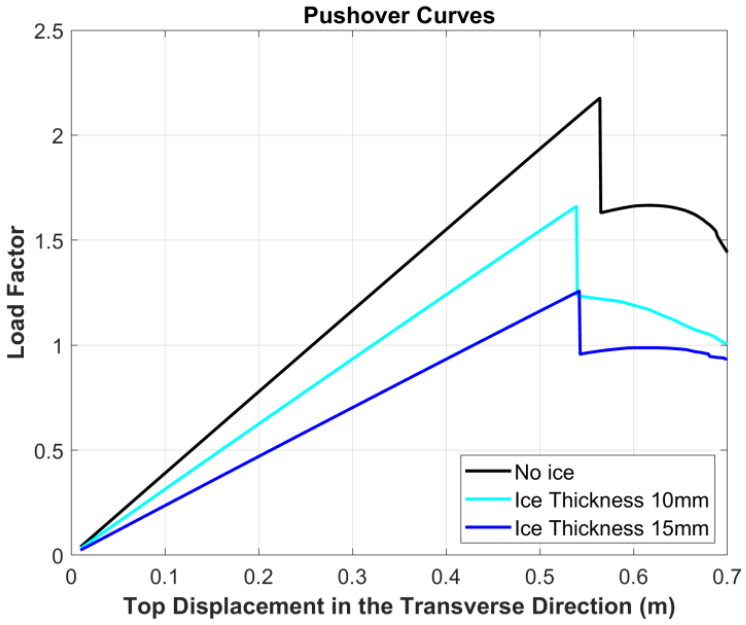

Figure 3.7: Pushover curves

3.3.4 Dynamic Analysis

Figure 3.8 presents the typical results of the dynamic analyses regarding the top displacements in the transverse direction of the line (along Y). The time history of the graph at the left corresponds to a wind time history (input of analysis) with mean wind speed equal to 25 m/s at 10m (i.e. basic wind speed) and wind angle transverse to the direction of the line assuming no ice conditions. On the other hand, the graph at the right corresponds to exactly the same time history of wind but assuming an ice layer of 10mm thickness accredited on the tower members, insulators and conductors. In both cases, the dynamic load was applied gradually during the first 30sec of the time history. It is evident that when ice is considered the displacement limit (red line in the graphs) as calculated by pushover analysis (Figure 3.7) was exceeded and thus a failure (collapse) was observed and the dynamic analysis was terminated.

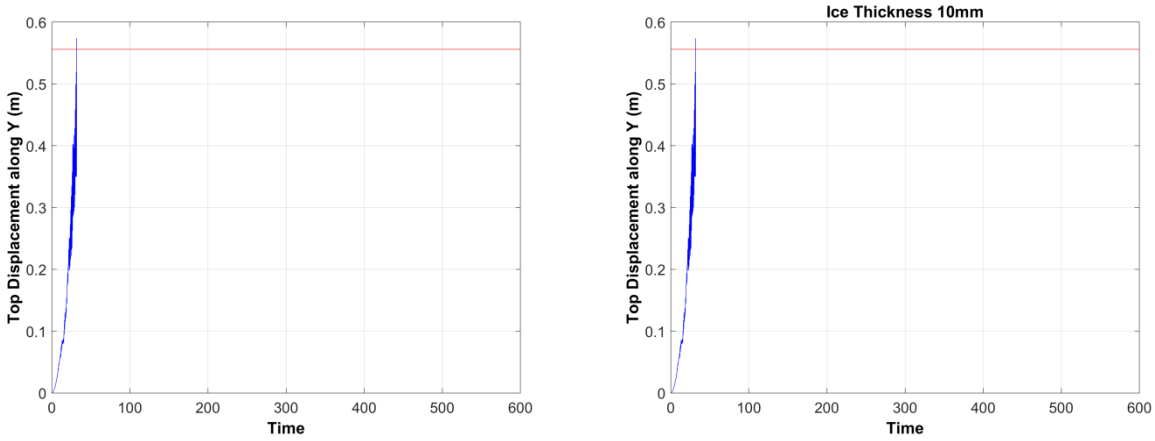

Figure 3.8: Typical time histories of top displacement in the transverse direction (along Y) of the initial suspension tower for mean wind speed equal to the basic wind speed (25 m/s)

3.4 Corroded Tower

3.4.1 Corrosion assumptions

The thickness loss of members due to corrosion was estimated following the same methodology as in the case of the telecommunication tower, described in Section 2.5.1. The environment of installation of the transmission tower was assumed to be of category C3 (medium corrosivity) according to [18]. The corresponding corrosion rates were assumed to be r_{av}=2μm/yr for the zinc and r_{av}=12μm/yr following be r_{lin}=6μm/yr for the carbon steel based on ISO 9224 [14].The thickness of the zinc layer was assumed to be equal of 40μm, thus it is expected to be exhausted during the first 20 years of service. The resulting carbon steel loss that will follow is presented in Figure 3.9. Finally, assuming a service life of 60 years, the estimated loss of thickness for carbon steel at the end of the service life is 0.3mm.

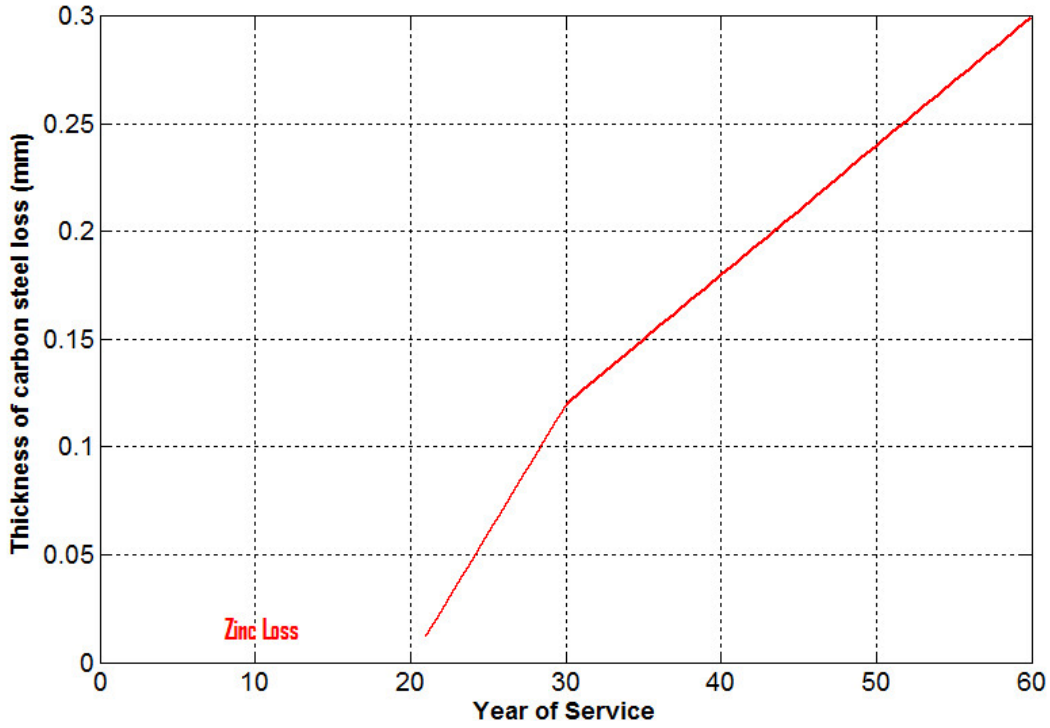

Figure 3.9: Loss of thickness during service life of the suspension transmission tower

3.4.2 Member sections

Based on the results of Figure 3.9, the final dimensions of cross-section for the members of initial tower in the corroded state assuming 60 years of service are presented in Table 3.3.

Table 3.3: Final dimensions of cross-section of the suspension tower in the corroded state

Initial Cross-Section	Corroded State		Initial Cross-Section	Corroded State	
	h=b (mm)	t (mm)		h=b (mm)	t (mm)
L150.150.13	149.4	12.4	L80.80.6	79.4	5.4
L150.150.12	149.4	12.4	L80.80.5	79.4	4.4
L140.140.15	139.4	14.4	L76.76.4.8	75.4	4.16
L130.130.8	129.4	7.4	L75.75.6	74.4	5.4
L120.120.16	119.4	15.4	L75.75.5	74.4	4.4
L120.120.7	119.4	6.4	L75.75.4	74.4	3.4
L100.100.7	99.4	6.4	L65.65.4	64.4	3.4
L90.90.6	89.4	5.4	L60.60.4	59.4	3.4
L90.90.5	89.4	4.4	L45.45.4	44.4	3.4
L80.80.10	79.4	9.4	L45.45.3	44.4	2.4

The smaller dimensions of cross-sections result in a reduction of the area of cross-section and the moments of inertia. This will reduce the strength of each member and will change the corresponding stress-strain curve (Figure 3.2).

Finally, it should be noted that in this work the conservative assumption that the projected areas of the members were not changed due to the effect of corrosion was made for the simplification of the calculations. Thus, the wind forces remain the same as in the case of the initial tower.

3.4.3 Eigenvalue Analysis

The natural periods of the corroded structure were determined by a modal analysis. They were slightly higher than those of the initial tower (Figure 3.5) as expected. This should be attributed to the lower moment of inertia and thus the lower stiffness of the corroded structure. Figure 3.10 presents the first three modes and the corresponding periods of the corroded tower assuming no ice accretion. The corresponding periods were estimated for the ice conditions and resulted in higher values.

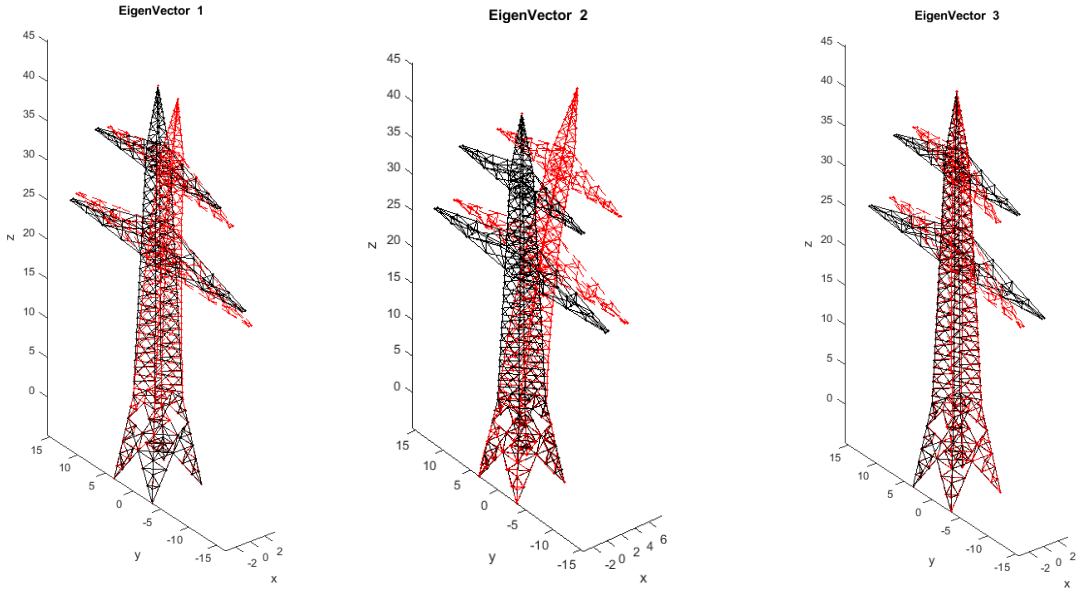

1st Mode	2nd Mode	3rd Mode
T_1=0.526 sec	T_2=0.517 sec	T_3=0.466 sec

Figure 3.10: First three modes and corresponding natural periods

3.4.4 Pushover Analysis

The pushover analysis of the corroded model (for no ice scenario) showed a similar pattern to that of the initial model. However, as shown in Figure 3.11, the maximum *LF* (where the failure occurs) was lower than the initial model and the top displacement at failure was also lower. The above findings are expected and should be attributed to lower strength of the corroded tower.

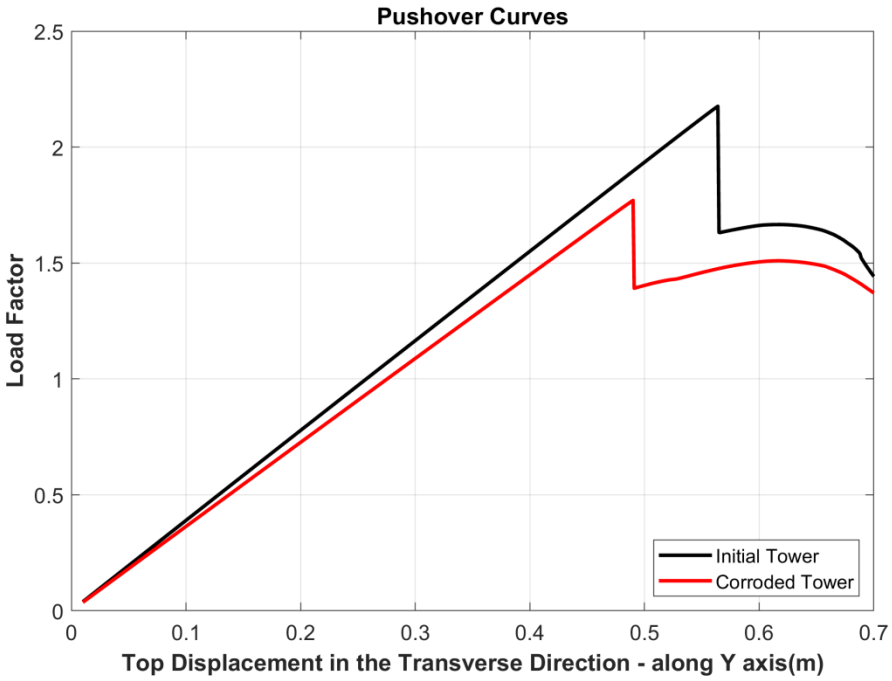

Figure 3.11: Pushover curves of the initial vs corroded suspension tower

3.4.5 Dynamic Analysis

Figure 3.12 presents the typical results of the dynamic analyses regarding the top displacements in the transverse direction of the line (along Y) for the case of the corrode model. The time history of the graph at the left corresponds to a wind time history (input of analysis) with mean wind speed equal to 25 m/s at 10m (i.e. basic wind speed) and wind angle transverse to the direction of the line assuming no ice conditions. On the other hand, the graph at the right corresponds to exactly the same time history of wind but assuming an ice layer of 10mm thickness accredited on the tower members, insulators and conductors. In both cases, the dynamic load was applied gradually during the first 30sec of the time history. Once again, as in the case of the initial model, when ice is considered the displacement limit (red line in the graphs) as calculated by pushover analysis (Figure 3.11) was exceeded and thus a failure (collapse) was observed and the dynamic analysis was terminated.

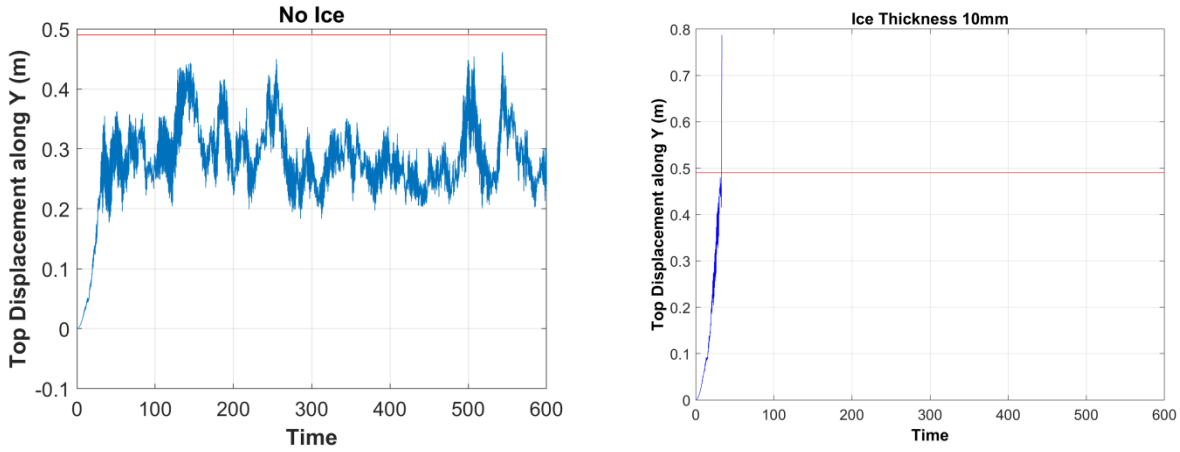

Figure 3.12: Typical time histories of top displacement in the transverse direction (along Y) of the corroded suspension tower for mean wind speed equal to the basic wind speed (25 m/s)

3.5 High Strength Steel member Tower

3.5.1 Redesign with High Strength Steel

As in the case of the telecommunication tower, a redesigned version of the initial suspension tower model with High Strength Steel (HSS) was also studied. The HSS tower had the same geometry with the initial one (Figure 3.4). Furthermore, two different grades were assumed. The angle profiles along with the corresponding steel grade for each of the group of members used in the HSS suspension tower are listed in Table 3.4.

The actual values for yielding and ultimate stresses for the used steel grades were adopted by [2]. In specific, for the S460 steel grade and cross-sections with thickness up to 15mm the actual yield stress was considered equal to 495.26 MPa and the ultimate stress equal to 620.98 MPa. For the same steel grade and thickness larger than 16mm the corresponding values were 521.10 MPa and 614.95 MPa, respectively. On the other hand, for S355 and thickness up to 15mm the yielding stress was considered equal to 414.09 MPa and the ultimate stress equal to 546.16 MPa, while for thickness larger than 15mm the corresponding values were 454.90 MPa and 546.84 MPa, respectively. Finally, it is noteworthy that the use of HSS steel angle profiles reduced the total weight of the structure by 1.0 ton.

Table 3.4: Angle profiles used for the members of the HSS suspension tower

Group	Angle Type	Angle Size	Steel grade
Bottom-legs	SAE	AM 140x140x12	S460M
Segment 2	SAE	AM 140x140x12	S460M
Segment 3	SAE	AM 100x100x16	S460M
Segment 4	SAE	AM 90x90x7-	S460M
Segment 5	SAE	AM 70x70x6-	S460M
Segment 6	SAE	AM 60x60x5	S460M
Segment 7	SAE	AM 45x45x3	S460M
Diagonal 1	SAE	AM 75x75x4	S355J2
Diagonal 2	SAE	AM 75x75x4	S355J2
Diagonal 3	SAE	AM 90x90x5	S355J2
Diagonal 4	SAE	AM 90x90x6	S355J2
Diagonal 5	SAE	AM 60x60x4	S355J2
Diagonal 6	SAE	AM 45x45x4	S355J2
Cross 1-bottom	SAE	AM 140x140x12	S460M
Cross 1-top	SAE	AM 120x120x7	S460M
Cross 1-base	SAE	AM 130x130x8	S460M
Horizontal 1	SAE	AM 80x80x5	S460M
Horizontal 2	SAE	AM 90x90x5	S460M
Horizontal 3	SAE	AM 90x90x7-	S460M
Horizontal 4	SAE	AM 75x75x4	S460M
Horizontal 5	SAE	AM 70x70x6-	S460M
Horizontal 6	SAE	AM 55x55x4	S460M
Horizontal 1 base	SAE	AM 76x76x4.8	S460M
Horizontal 2 base	SAE	AM 80x80x5	S460M
Horizontal 3 base	SAE	AM 76x76x4.8	S460M
Horizontal 4 base	SAE	AM 60x60x4	S460M
Cross - Horizontal	SAE	AM 45x45x3	S355J2
Cross 2-bottom	SAE	AM 110x110x7	S460M
Cross 2-top	SAE	AM 75x75x5	S460M
Cross 2-base	SAE	AM 90x90x5	S460M
Redundant 1	SAE	AM 90x90x5	S355J2
Redundant 2	SAE	AM 60x60x4	S355J2
Redundant 3	SAE	AM 90x90x5	S355J2

3.5.2 Eigenvalue Analysis

Figure 3.13 presents the first three modes and the corresponding periods of the HSS tower assuming no ice accretion. The values of the eigenperiods are lower than the corresponding values of the initial model, a fact that could be attributed to the lower weight of the structure.

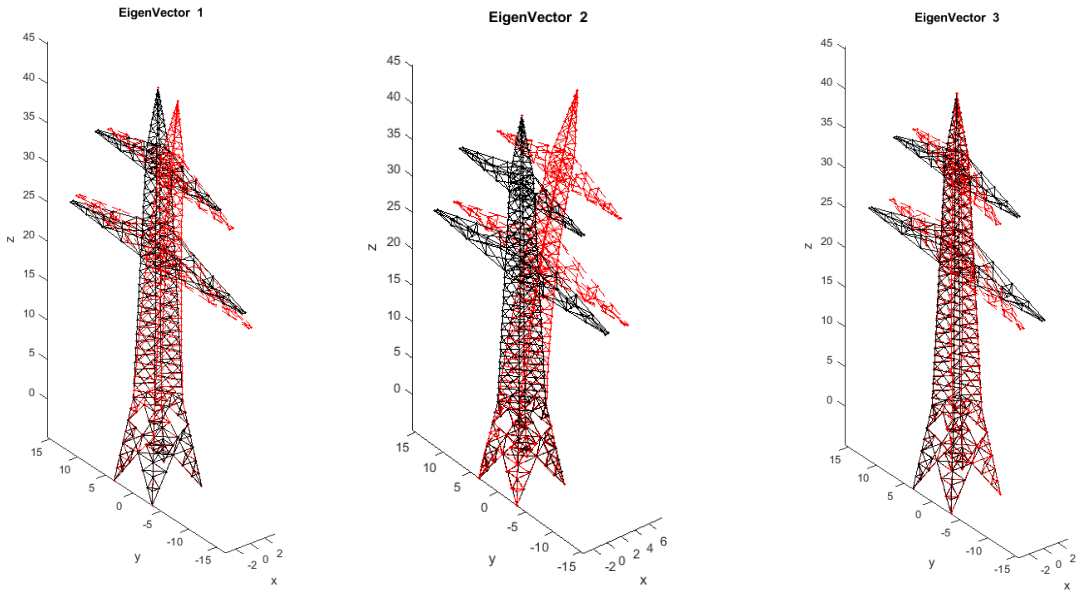

1st Mode
T_1=0.500 sec

2nd Mode
T_2=0.494 sec

3rd Mode
T_3=0.426 sec

Figure 3.13: First three modes and corresponding natural periods of the HSS suspension tower

3.5.3 Pushover Analysis

Figure 3.14 shows the pushover curve (blue line) for the HSS suspension tower. Furthermore, the corresponding pushover curves of the initial and the corroded version of the tower are presented for the sake of comparison.

The *LF* when the first failure occurs is slightly lower than that of the initial model and the top displacement at the time of first failure is larger than any of the other models and equal 0.642m.

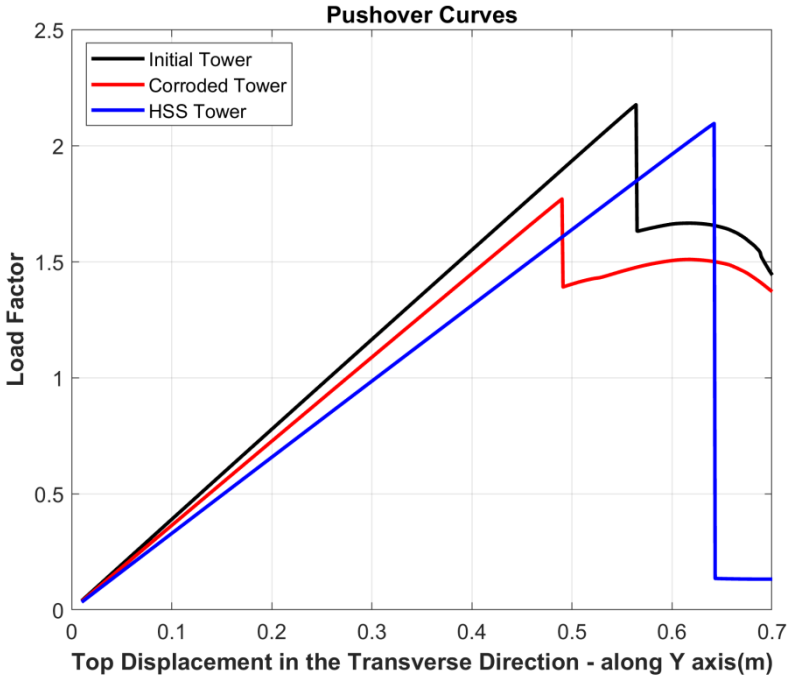

Figure 3.14: Pushover curves of the three versions of suspension transmission towers

3.5.4 Dynamic Analysis

Figure 3.15 presents the typical results of the dynamic analyses regarding the top displacements in the transverse direction of the line (along Y) for the case of the corrode model. The time history of the graph at the left corresponds to a wind time history (input of analysis) with mean wind speed equal to 25 m/s at 10m (i.e. basic wind speed) and wind angle transverse to the direction of the line assuming no ice conditions. On the other hand, the graph at the right corresponds to exactly the same time history of wind but assuming an ice layer of 10mm thickness accredited on the tower members, insulators and conductors. In both cases, the dynamic load was applied gradually during the first 30sec of the time history. Once again, as in the case of the initial model, when ice is considered the displacement limit (red line in the graphs) as calculated by pushover analysis (Figure 3.11) was exceeded and thus a failure (collapse) was observed and the dynamic analysis was terminated.

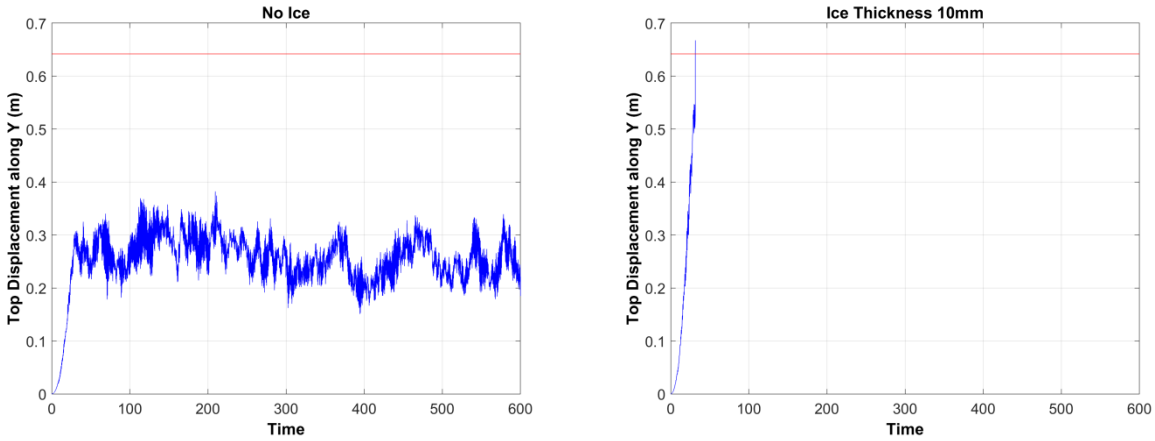

Figure 3.15: Typical time histories of top displacement in the transverse direction (along Y) of the HSS suspension tower for mean wind speed equal to the basic wind speed (25 m/s)

4 Dead-End Power Transmission Tower

4.1 Structural description and modelling

4.1.1 Geometry

The Dead-End transmission tower of study has exactly the same geometry and is discretised in the same number of segments as the suspension tower (Figure 4.1). The tower carries two 380kV circuits, each of them consisting of three phases. Each phase is made of a bundle of four conductors supported by two insulators hanging horizontally. The type of insulators is assumed to be the same with those used in the suspension tower with a weight of 87N (i.e. 9 Kg) each.

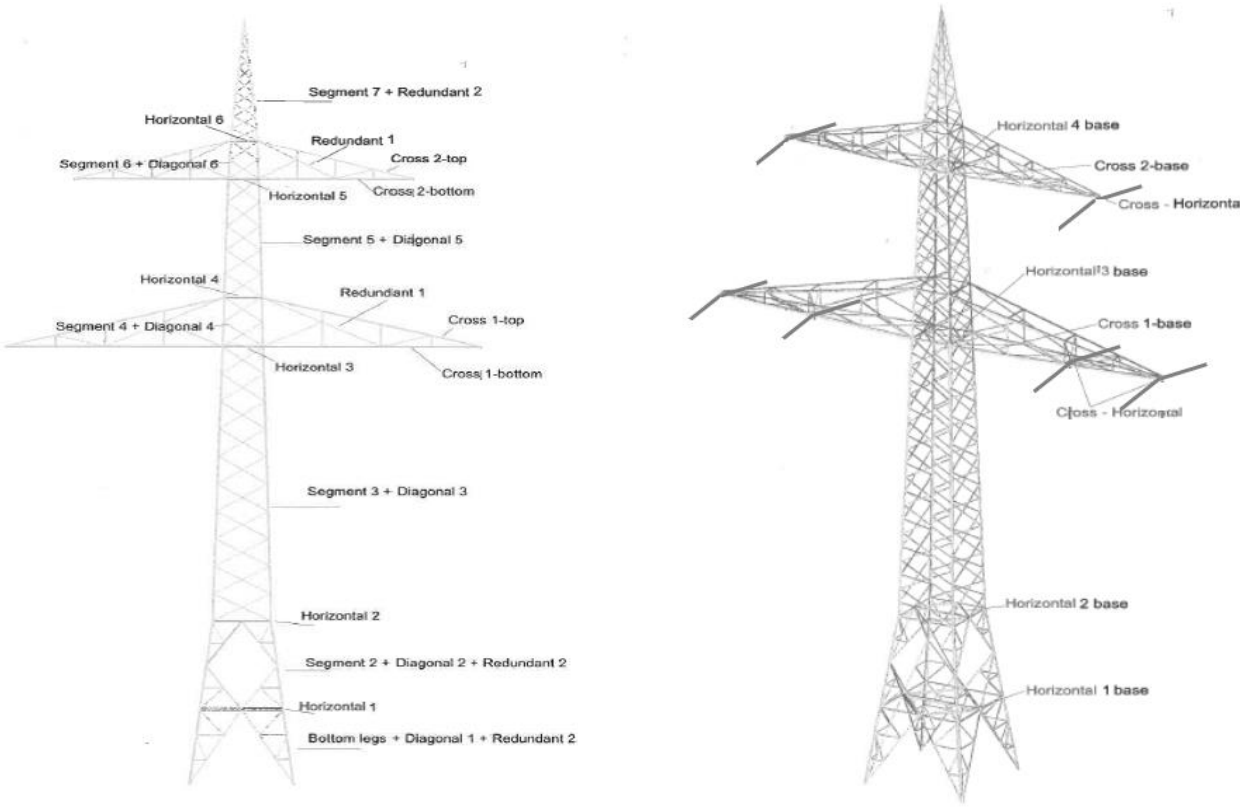

Figure 4.1: Dead-End transmission tower configuration

4.1.2 Material

As in the case of the suspension tower, fiber sections were employed together with beam-column and truss elements create the Finite Element Model. Furthermore, to assign stress-strain relationships to each steel fiber, the general form of Figure 4.2 was employed as stress-strain curve in compression and tension, using the buckling reduction factor χ, as calculated for each structural member according to EN 1993-3-1 [3], to account for compression buckling. In all cases, the actual values for yielding (f_y) and ultimate stresses (f_u) of the corresponding steel grades were used as provided by [2]. The modulus of elasticity of steel was taken as E=210GPa.

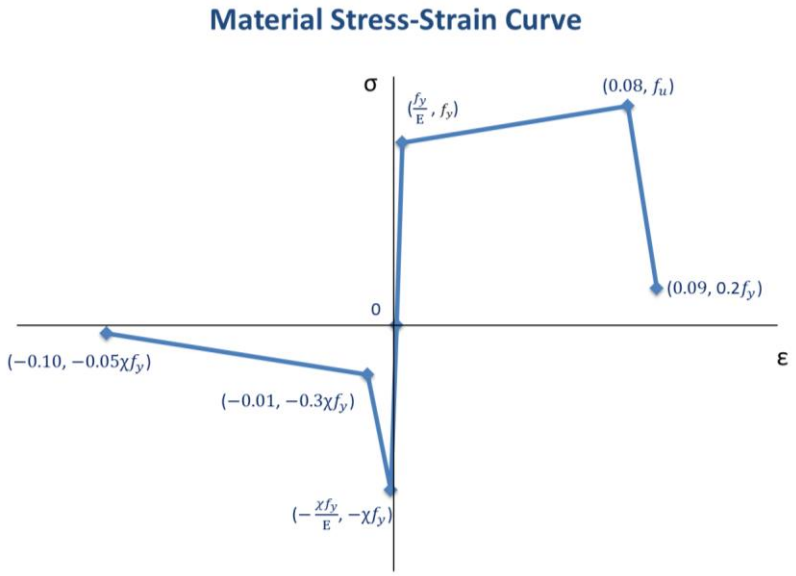

Figure 4.2: General form of a member stress-strain curve

4.2 Loads

4.2.1 Gravity Loads

The total weight of all tower members was calculated after multiplying the length of each member by the corresponding unit weight of the member's angle profile. For each of the twelve insulators considered in the model the weight was estimated to be 87N, resulting in a total weight of 1044N (i.e. 106.46kg).

4.2.2 Wind Loads at the tower

The wind force acting on the transmission tower is calculated following a similar process as described in Section 2.2.2.1 for the telecommunication antenna. For the calculations, each of the segments of the tower (Figure 4.1) was divided into sub-segments of approximately 1.5 m height. Then, the solidity ratio φ of each sub-segment was calculated and the resulting wind force was estimated using Eq. (2.2) and considering the corresponding wind speed for each sub-segment based on its height. Finally, the wind force was assigned to the corner nodes of each sub-segment.

4.2.2.1 Wind Speed Profile and Wind Field Simulation

A similar process as described in Section 2.2.2.3 was applied for the estimation of the wind speed values (i.e. wind profile) along the height of the tower using the same assumptions as in the case of the telecommunication antenna.

The TurbSim software was also used for the wind field simulation. However, in this case the simulated wind field had a width equal 2100 in order to simulate the wind speeds along the whole power line's length which was assumed to be equal to 2100m, consisting of six spans of 350m length each. The calculations for estimating the conductors' forces will be described in Section 4.2.4.

4.2.3 Ice Loads on tower

The ice loads were estimated by assuming ice layer of uniform thickness accumulated on the exposed surfaces of the tower members following the process described in Section 2.2.3. Finally, a number of scenarios of various ice thicknesses were applied as in the case of the telecommunication antenna.

4.2.4 Conductor and Insulator Loads

A dead-end tower can carry not only vertical and transverse loads (as a suspension tower) but also tension (i.e. longitudinal) loads of the conductors strained in its horizontal strain insulators. Thus, for the case of the dead-end tower, apart from transverse, vertical loads and insulator loads that are estimated following the methodology of Section 3.2.4, the longitudinal loads due to conductors should be applied on the cross-arms of the dead-end tower.

A simple way to transfer the longitudinal loads to the dead-end towers along a power line is to model the line as a continuous beam with supports at the points of the dead-end towers. Herein, a power line with six spans (with a length of 350m each) with three dead-end towers (shown in red) and four suspension towers (shown in green) is assumed (Figure 4.3).

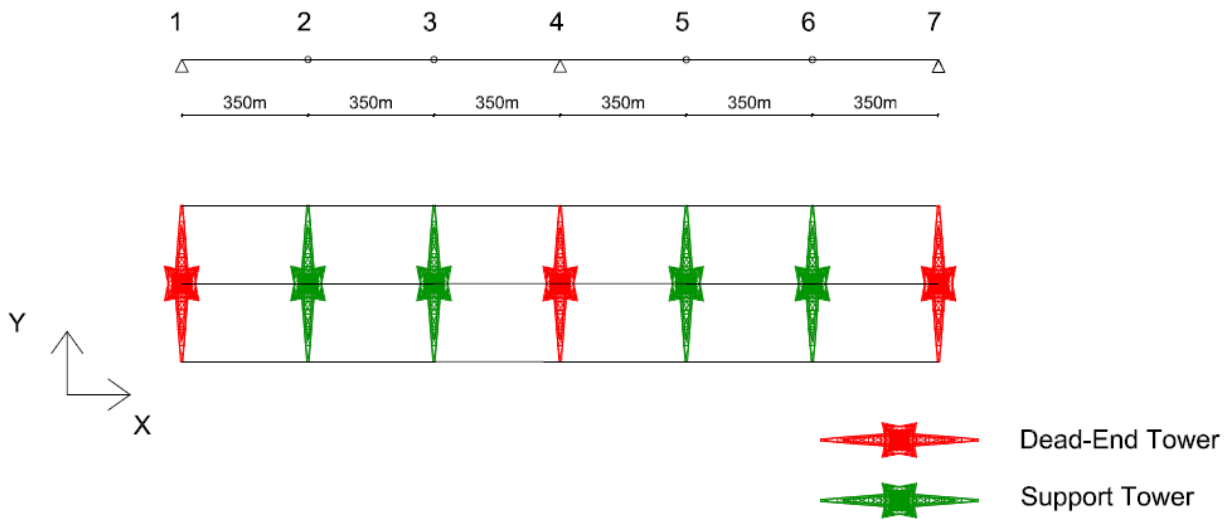

Figure 4.3: Full Power Line Model

The stiffness of each span is estimated according to [25] as follows:

$$k_c = \frac{1}{1+\rho}\frac{AE}{L_e}\cos^2\theta + \frac{T_o}{L}\sin^2\theta \qquad \text{Eq. 4.1}$$

$$\rho = \frac{1}{12}\frac{AE}{T_o}\frac{L}{L_e}\left(\frac{q_y L}{T_o}\right)^2 \qquad \text{Eq. 4.2}$$

where:

A and E are the cross-sectional area and the elastic modulus of the conductor, respectively, θ is the inclination angle of the conductor, T_o is the conductor's tension, L_e is the effective length equals to $L \times \left[1 + 8 \times \left(\frac{sag}{L}\right)^2\right]$, where L is the span length and q_y is the normal load per unit of conductor's length.

In the present work the focus will be on the dead-end tower of point 4 (Figure 4.3). In order to estimate the conductor longitudinal forces transferred to point 4, one could break the line into two pieces (at left and right of point 4) and estimate the reactions of each piece at point 4 (R_4^{left} and

R_4^{right}). The forces F_i of Figure 4.4 correspond to the longitudinal components of tensions due to conductors at each suspension tower, which are transferred to dead-end towers.

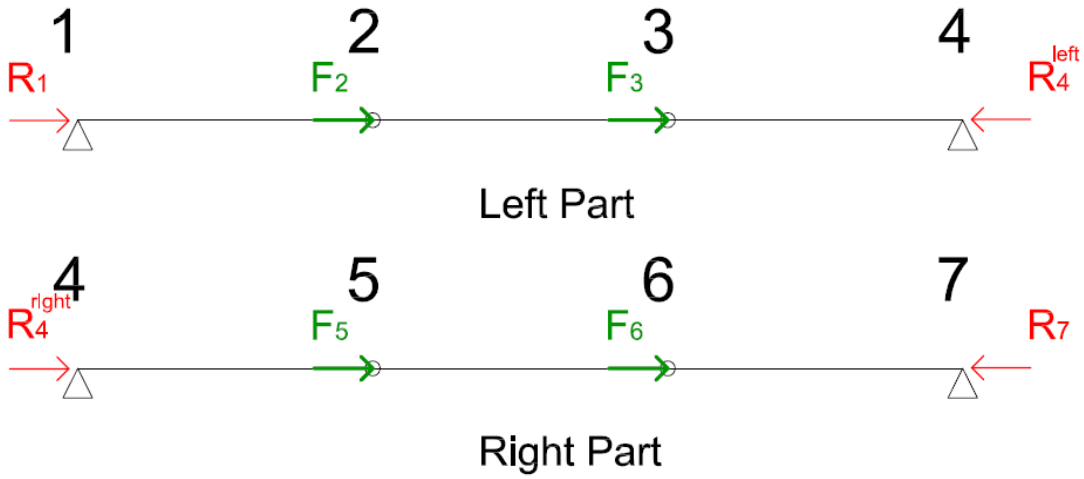

Figure 4.4: Longitudinal components of forces due conductors transferred to dead end towers

The total longitudinal force at dead-end tower of point 4 is estimated by the equation:

$$\overrightarrow{R_4} = \overrightarrow{R_4^{left}} + \overrightarrow{R_4^{right}} \qquad \text{Eq. 4.3}$$

Finally, it should be noted that the above estimation of Eq. (4.3) is performed for each time-step of the simulated wind time histories. Furthermore, as stated in Section 4.2.2.1, the simulated full field should have a length equal to the full length of the line (herein 2100m).

4.3 Initial Tower

4.3.1 Member sections

As in the case of the suspension tower, all members of the dead-end tower were composed from equal leg angles of various sizes listed in Table 4.1. Furthermore, the members were grouped in various groups according to their size and location in the tower as shown in Figure 4.1.

Table 4.1: Angle profiles used for the members of the dead-end tower

Group	Angle Type	Angle Size	Steel grade
Bottom-legs	DAE	AM 300x300x35	S355J2
Segment 2	DAE	AM 300x300x35	S355J2
Segment 3	SAE	AM 300x300x35	S355J2
Segment 4	SAE	AM 180x180x16-/+	S355J2
Segment 5	SAE	AM 150x150x15-/+	S355J2
Segment 6	SAE	AM 90x90x5	S355J2
Segment 7	SAE	AM 60x60x5	S355J2
Diagonal 1	SAE	AM 150x150x10-/+	S355J2
Diagonal 2	SAE	AM 140x140x12	S355J2
Diagonal 3	SAE	AM 160x160x15+	S355J2
Diagonal 4	SAE	AM 120x120x8	S355J2
Diagonal 5	SAE	AM 130x130x8	S355J2
Diagonal 6	SAE	AM 55x55x4	S355J2
Cross 1-bottom	SAE	AM 250x250x17	S355J2
Cross 1-top	SAE	AM 120x120x8	S355J2
Cross 1-base	SAE	AM 150x150x12-/+	S355J2
Horizontal 1	SAE	AM 80x80x5	S355J2
Horizontal 2	SAE	AM 130x130x9	S355J2
Horizontal 3	SAE	AM 160x160x16-/+	S355J2
Horizontal 4	SAE	AM 75x75x4	S355J2
Horizontal 5	SAE	AM 150x150x12-/+	S355J2
Horizontal 6	SAE	AM 65x65x4	S355J2
Horizontal 1 base	SAE	AM 80x80x5	S355J2
Horizontal 2 base	SAE	AM 80x80x5	S355J2
Horizontal 3 base	SAE	AM 120x120x9	S355J2
Horizontal 4 base	SAE	AM 100x100x7	S355J2
Cross - Horizontal	SAE	AM 75x75x7	S355J2
Cross 2-bottom	SAE	AM 180x180x14+	S355J2
Cross 2-top	SAE	AM 90x90x5	S355J2
Cross 2-base	SAE	AM 130x130x9	S355J2
Redundant 1	SAE	AM 90x90x5	S355J2
Redundant 2	SAE	AM 90x90x6	S355J2
Redundant 3	SAE	AM 90x90x5	S355J2

4.3.2 Eigenvalue Analysis

The natural frequencies of the structure were determined by modal analysis. The first two modes are longitudinal (directions Y and X) and the third mode is torsional (Figure 4.5). The resulting eigenperiods of the dead-end tower are lower than the corresponding eigenperiods of the suspension tower (Figure 3.5) indicating that the dead-end power is stiffer than the suspension tower.

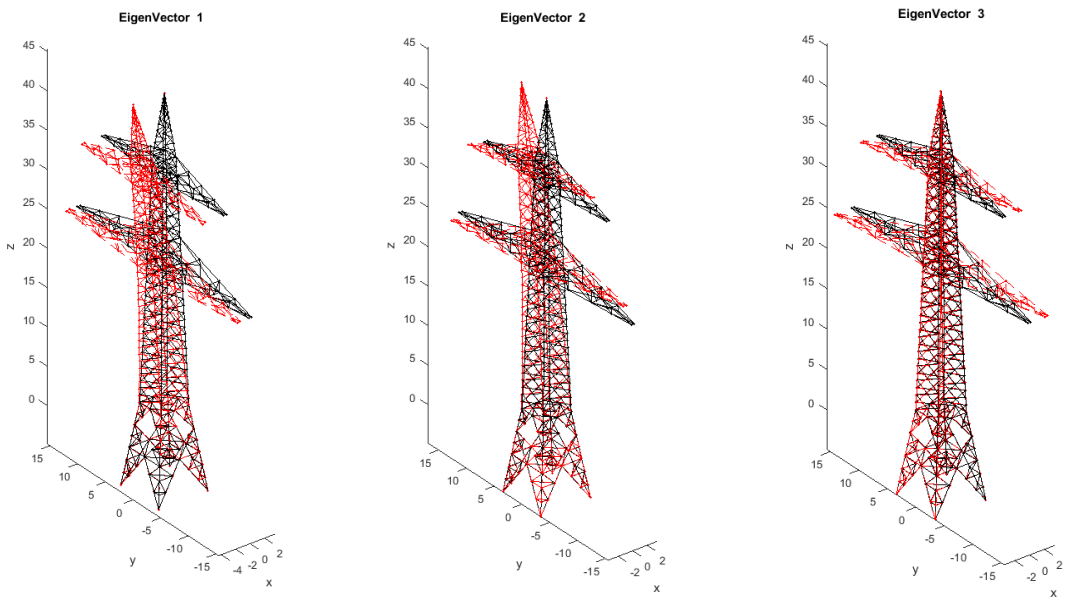

1st Mode
T_1=0.371 sec

2nd Mode
T_2=0.370 sec

3rd Mode
T_3=0.368 sec

Figure 4.5: First three modes and corresponding natural periods of the initial dead-end tower

Modal analyses were also performed for each of the icing scenarios. Table 4.2 presents the periods of the first three modes for each of the various scenarios considered herein. The results show, similarly to the cases of the telecommunication and the suspension tower, that as the thickness of the ice layer increases, the corresponding periods increase.

Table 4.2: Natural periods of the first three modes for various icing scenarios

Ice Thickness (mm)	T_1 (sec)	T_2 (sec)	T_3 (sec)
1	0.375	0.374	0.372
10	0.410	0.408	0.404
15	0.427	0.425	0.421

4.3.3 Pushover Analysis

As in the cases of telecommunication and suspension transmission towers, the first step, before the nonlinear dynamic analysis, was to perform a pushover (nonlinear static) analysis in order to understand the failure mechanisms of the tower. A lateral load profile transverse to the direction of the line is considered following the power-law pattern of the wind speed. Pushover analysis was conducted for various scenarios of icing. The results show that the first failure occurs at the segment of the tower between the two cross-arms (Figure 4.6).

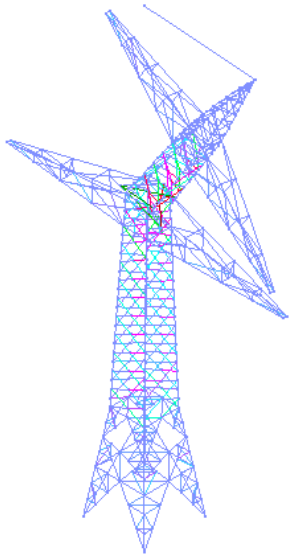

Figure 4.6: Failure mode of dead-end tower as revealed by pushover analysis pushover analysis

Figure 4.7 presents the pushover curves for various icing scenarios. The horizontal axis depicts the displacement of the top of the tower along the lateral load direction (transverse to the transmission line), while the vertical axis depicts the Load Factor (LF). A Load Factor equal to 1 (*LF=1*) corresponds to the load caused by a wind speed at a height of 10m equal to the basic wind speed used in the design, i.e. 25 m/s. For example, at the no ice scenario, the failure occurs when the top displacement in the direction transverse to the transmission line reaches 0.684m. At this point the LF is about 12.23 which means that the lateral loads at the time of the first member failure is 12.23 times larger than the lateral loads that correspond to a reference wind speed of 25 m/s at 10m. Figure 4.7 also shows that as the thickness of the ice layer on the structure and conductors increases, the first failure occurs in lower LF values.

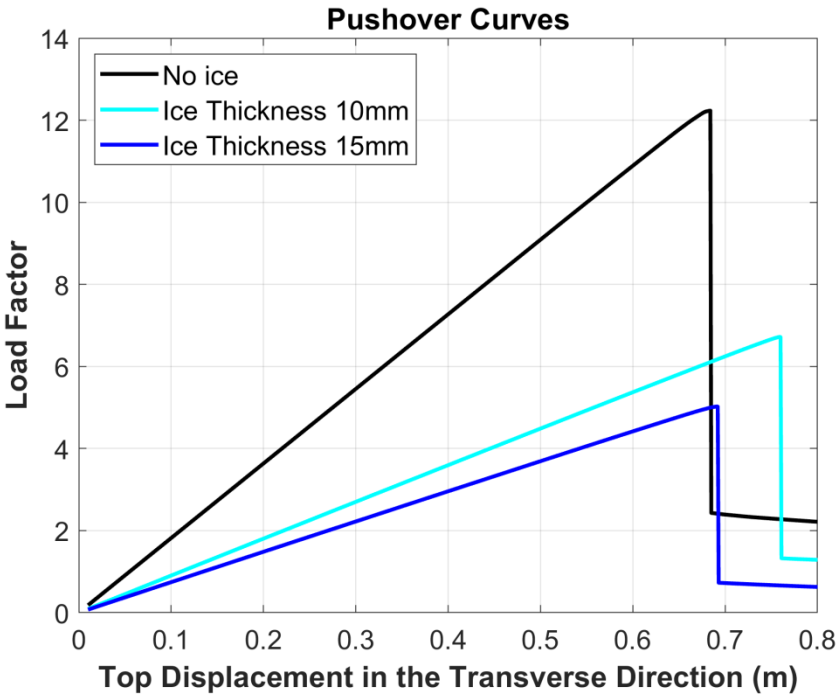

Figure 4.7: Pushover curves for dead-end tower

4.3.4 Dynamic Analysis

Figure 4.8 presents the typical results of the dynamic analyses regarding the top displacements in the transverse direction of the line (along Y). The time history of the graph at the left corresponds to a wind time history (input of analysis) with mean wind speed equal to 25 m/s at 10m (i.e. basic wind speed) and wind angle transverse to the direction of the line assuming no ice conditions. On the other hand, the graph at the right corresponds to exactly the same time history of wind but assuming an ice layer of 10mm thickness accredited on the tower members, insulators and conductors. The dynamic load was applied gradually during the first 30sec of the time history. In both cases the resulting top displacements were much lower than the failure limit from pushover for (Figure 4.7) and thus no failure was observed. Moreover, one could infer that a wind speed much larger than the basic wind speed of design is needed in order to observe a failure. Indeed, even for a time history with mean wind speed of 55m/s as in Figure 4.9, the dead-end tower is expected to fail only when 10mm ice will be accreted on the tower members and the conductors.

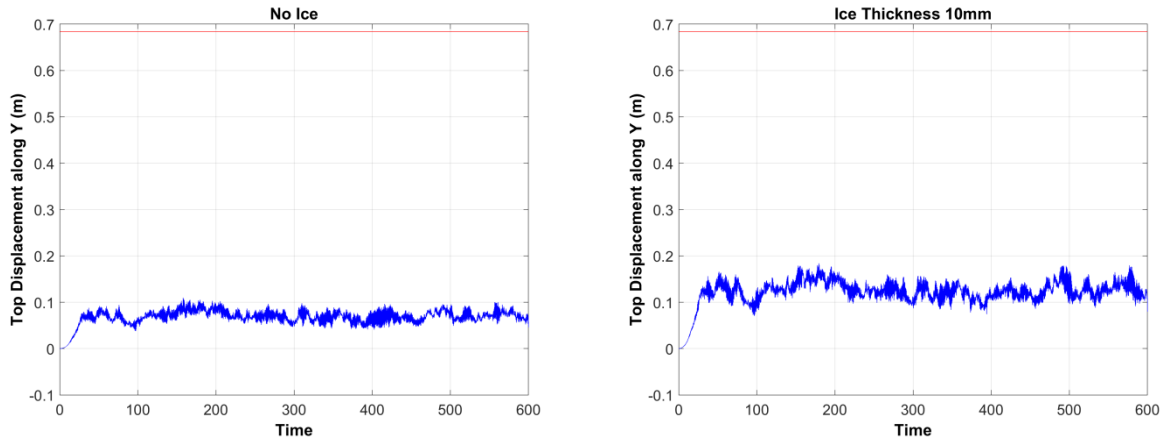

Figure 4.8: Typical time histories of top displacement in the transverse direction (along Y) of the initial dead-end tower for mean wind speed equal to the basic wind speed (25 m/s)

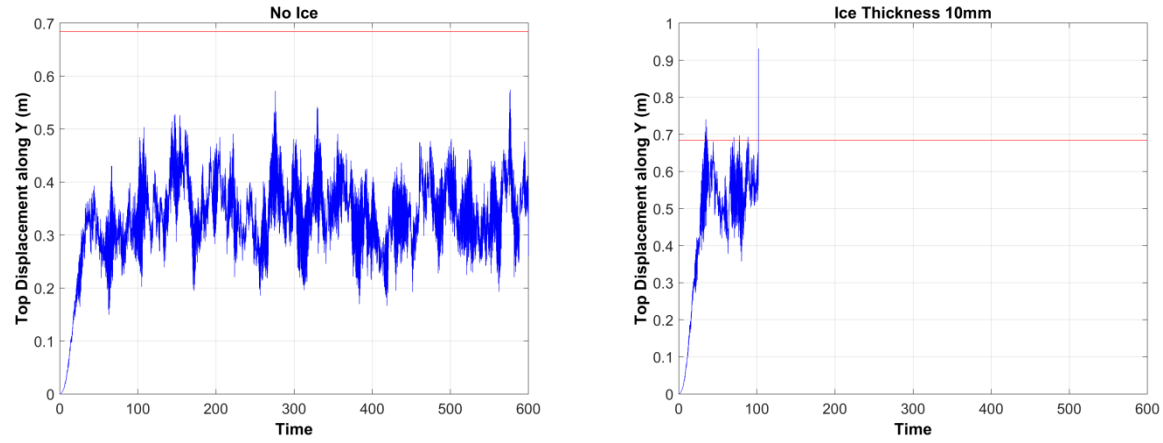

Figure 4.9: Time histories of top displacement in the transverse direction (along Y) of the initial dead-end tower for a mean wind speed of 55 m/s

4.4 Corroded Tower

4.4.1 Corrosion assumptions

The thickness loss of members due to corrosion was estimated following the same methodology as in the case of the telecommunication tower and the suspension transmission towers, described in Sections 2.5.1 and 3.4.1. The dead-end tower was assumed to be installed in similar environmental conditions of medium corrosivity (category C3 [18]) with the suspension tower. Thus, the corresponding corrosion rates for zinc and carbon steel as listed in Section 4.4.1. The predicted loss of thickness for carbon steel over the service life of the tower is presented in Figure 4.10. At the end of the service life the total loss of thickness of carbon steel will be equal to 0.3mm.

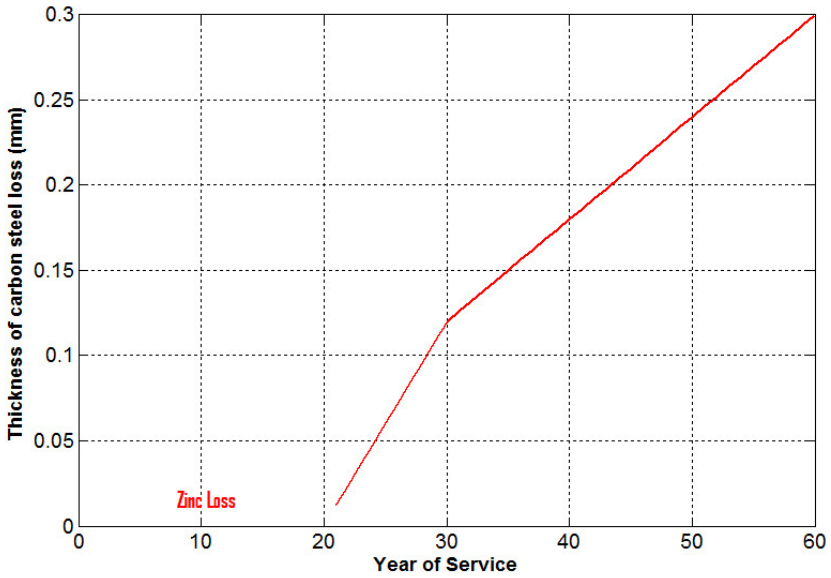

Figure 4.10: Loss of thickness during service life of the dead-end transmission tower

4.4.2 Member sections

Based on the results of Figure 4.10, the final dimensions of cross-section for the members of initial tower in the corroded state assuming 60 years of service are presented in Table 4.3.

Table 4.3: Final dimensions of cross-section of the dead-end tower in the corroded state

Initial Cross-Section	Corroded State		Initial Cross-Section	Corroded State	
	h=b (mm)	t (mm)		h=b (mm)	t (mm)
L300.300.35	299.4	34.4	L120.120.9	119.4	8.4
L250.250.17	249.4	16.4	L120.120.8	119.4	7.4
L180.180.16	179.4	15.4	L100.100.7	99.4	6.4
L180.180.14	179.4	13.4	L90.90.6	89.4	5.4
L160.160.16	159.4	15.4	L90.90.5	89.4	4.4
L160.160.15	159.4	14.4	L80.80.5	79.4	4.4
L150.150.15	149.4	14.4	L75.75.7	74.4	6.4
L150.150.12	149.4	11.4	L75.75.4	74.4	3.4
L150.150.10	149.4	9.4	L65.65.4	64.4	3.4
L140.140.12	139.4	11.4	L60.60.5	59.4	4.4
L130.130.9	129.4	8.4	L55.55.4	54.4	3.4
L130.130.8	129.4	7.4			

The smaller dimensions of cross-sections result in a reduction of the area of cross-section and the moments of inertia. This will reduce the strength of each member and will change the corresponding stress-strain curve (Figure 4.2).

Finally, it should be noted that in this work the conservative assumption that the projected areas of the members were not changed due to the effect of corrosion was made for the simplification of the calculations. Thus, the wind forces remain the same as in the case of the initial tower.

4.4.3 Eigenvalue Analysis

The natural periods of the corroded structure were determined by a modal analysis. They were slightly higher than those of the initial tower (Figure 4.5) as expected. This should be attributed to the lower moment of inertia and thus the lower stiffness of the corroded structure. Figure 4.11 presents the first three modes and the corresponding periods of the corroded tower assuming no ice accretion.

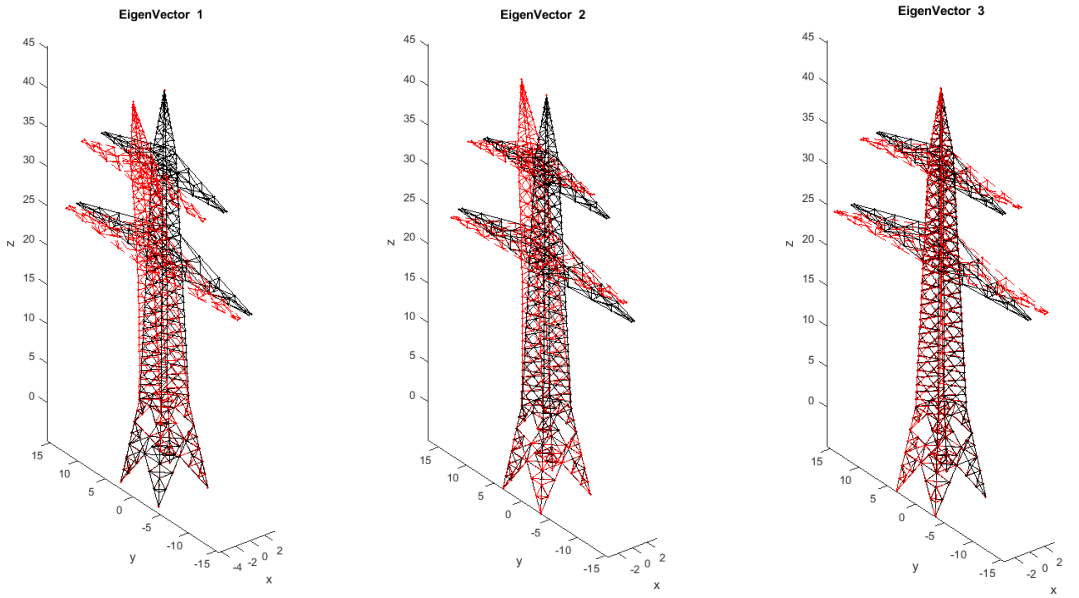

1st Mode
T_1=0.381 sec

2nd Mode
T_2=0.375 sec

3rd Mode
T_3=0.372 sec

Figure 4.11: First three modes and corresponding natural periods of the corroded dead-end tower

4.4.4 Pushover Analysis

The pushover analysis of the corroded model (for no ice scenario) showed a similar pattern to that of the initial model. However, as shown in Figure 4.12, the maximum *LF* (where the failure occurs) was lower than the initial model and the top displacement at failure was also lower. The above findings are similar to the case of the suspension tower and should be attributed to lower strength of the corroded tower.

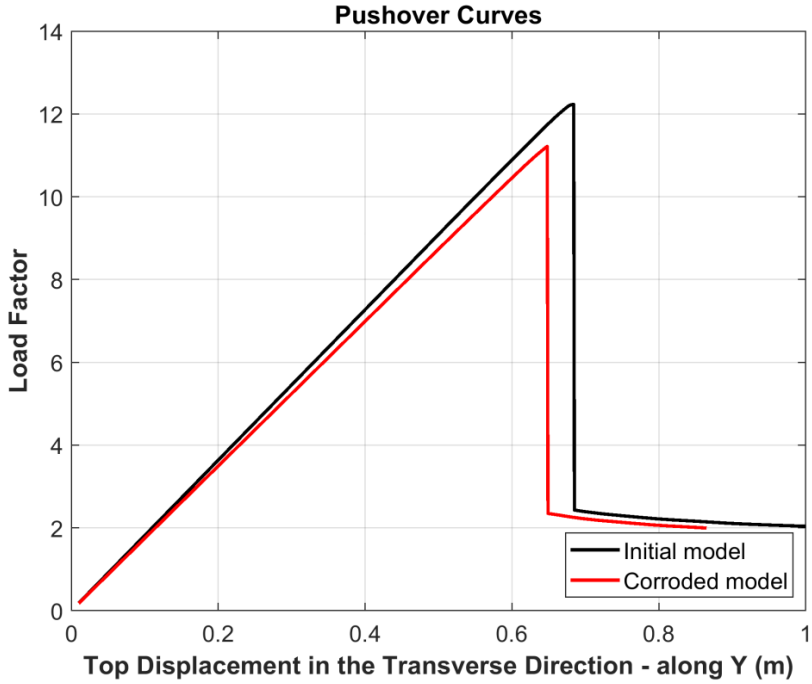

Figure 4.12: Pushover curves of the initial vs corroded dead-end tower

4.4.5 Dynamic Analysis

Figure 4.13 presents the typical results of the dynamic analyses regarding the top displacements in the transverse direction of the line (along Y). The time history of the graph at the left corresponds to a wind time history (input of analysis) with mean wind speed equal to 25 m/s at 10m (i.e. basic wind speed) and wind angle transverse to the direction of the line assuming no ice conditions. On the other hand, the graph at the right corresponds to exactly the same time history of wind but assuming an ice layer of 10mm thickness accredited on the tower members, insulators and conductors. The dynamic load was applied gradually during the first 30sec of the time history. In both cases the resulting top displacements were much lower than the failure limit from pushover for the corroded dead-end tower (Figure 4.12) and thus no failure was observed. Moreover, one could infer that a wind speed much larger than the basic wind speed of design is needed in order to observe a failure. Indeed, even for a time history with mean wind speed of 55m/s as in Figure 4.14, the dead-end tower is expected to fail only when 10mm ice will be accreted on the tower members and the conductors. The above findings are consistent with those of the case of the initial tower.

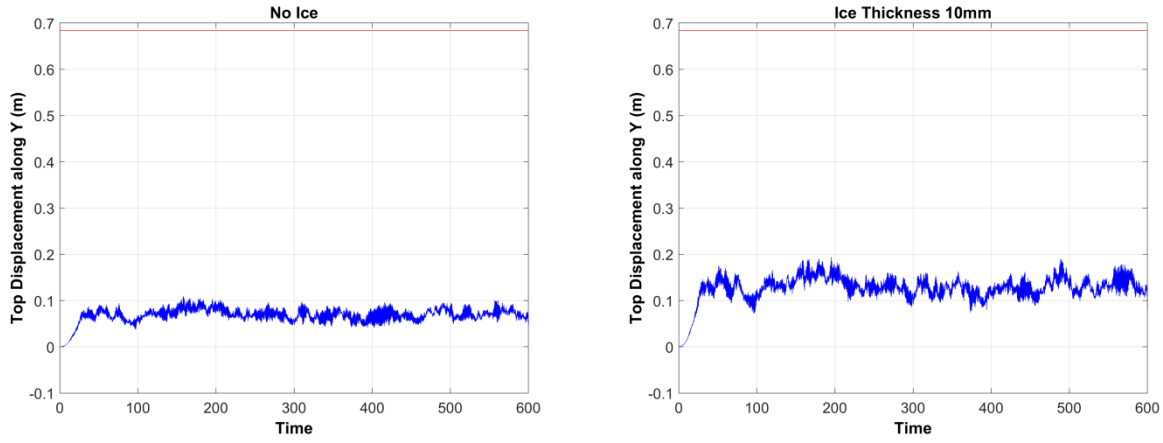

Figure 4.13: Typical time histories of top displacement in the transverse direction (along Y) of the corroded dead-end tower for mean wind speed equal to the basic wind speed (25 m/s)

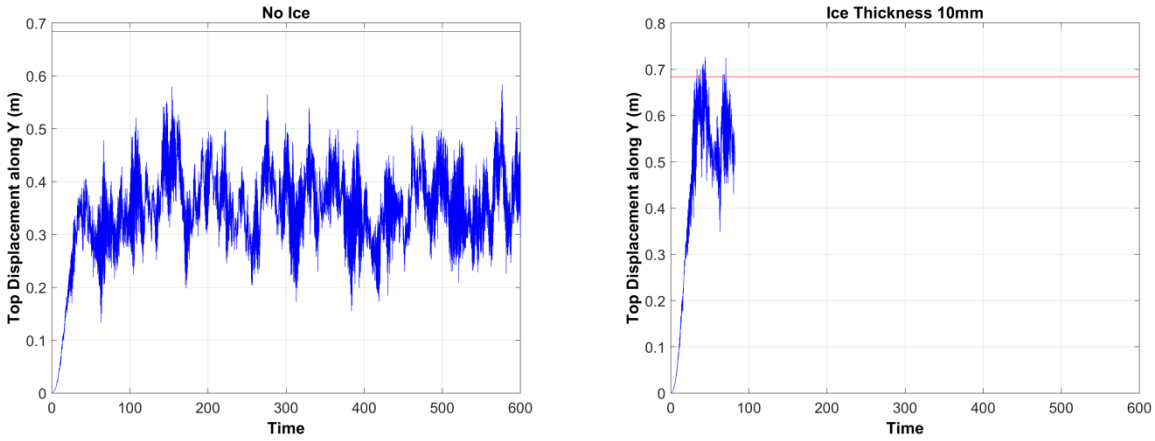

Figure 4.14: Time histories of top displacement in the transverse direction (along Y) of the corroded dead-end tower for a mean wind speed of 55 m/s

4.5 Strengthened Hybrid Member Tower

4.5.1 Strengthening methodology

The same innovative strengthening method using FRP plates, described in section 2.6.1, was applied also on the existing Dead-end transmission tower. The same FRP material as for telecommunication tower's strengthening was considered. Material properties are included in Table 2.3. Similar also to telecommunication tower, FRP plates are assumed to be placed externally on both legs of the existing angle section and only on the main tower's members, legs or primary braces in selected parts of the tower. Depending on the angle's size, several types of FRP plates can be used as shown in Table 4.5. Calculation of tension and buckling resistance of strengthened-hybrid members is analytically described in Deliverable 4.4 (Design guide) [19]. Regarding the angle steel section, cross-section properties were considered for members in the corroded state (see 4.4.2). In numerical simulations, the hybrid cross-section was transformed into an equivalent steel section with the mechanical properties of the hybrid section.

Table 4.4: FRP plates used for strengthening tower's members

Type of member	Existing angle section	Appropriate FRP plate
Diagonal, Segment 6	**L55.4**	**S 512 (b=50mm, t=1.2)**
Leg, Segment 6	**L90.5**	**S 812 (b=80mm, t=1.2)**
Diagonal, Segment 4	**L120.8**	**S 1012 (b=100mm, t=1.2)**
Diagonal, Segment 5	**L130.8**	**S 1012 (b=100mm, t=1.2)**

4.5.2 Strengthened Members

As in the case of the corroded telecommunication tower (Section 0), strengthening with FRP plates was selected for the members of the most vulnerable part ("sensitive area") of the corroded dead-end tower. The "sensitive area" was actually Segment 4 of the tower which is at the level of Cross Arm 1 (Figure 4.15 left). In specific only the diagonal (bracing) members of that Segment were selected for strengthening (Figure 4.15 right). It is noteworthy that except of strengthening only the diagonals of Segment 4, other scenarios of strengthening additional segments (such as Segments 5 and 6) were examined. However, strengthening additional members than only those of Segment 4

did not provide any considerable additional strength. Thus, under a cost-benefit perspective (i.e. having the same benefit in strength with the lowest cost), strengthening only the diagonals of Segment 4 was selected.

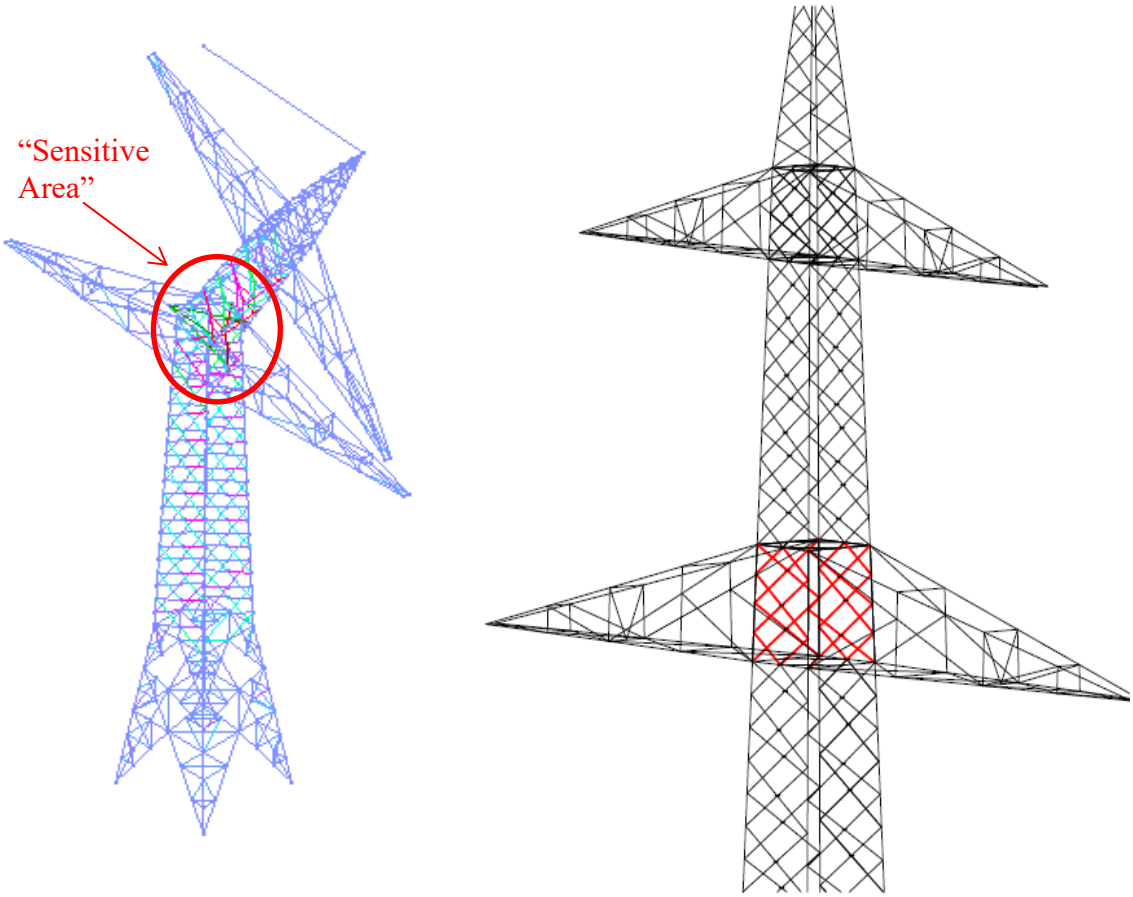

Figure 4.15: Area of strengthening corroded dead-end tower members with FRP stripes ("Sensitive Area")

4.5.3 Eigenvalue Analysis

Figure 4.16 presents the first three modes and the corresponding periods of the strengthened hybrid tower assuming no ice accretion. The values of the first two eigenperiods are higher than those of the initial towers and slightly lower than those of the corroded tower.

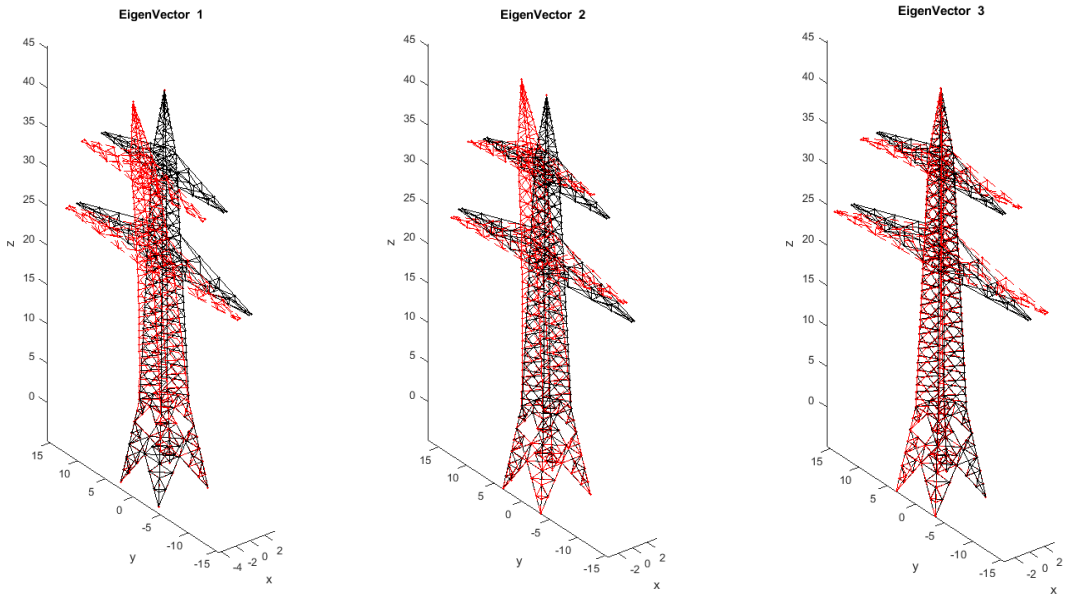

1st Mode
$T_1=0.380sec$

2nd Mode
$T_2=0.375\ sec$

3rd Mode
$T_3=0.372\ sec$

Figure 4.16: First three modes and corresponding natural periods of the strengthened hybrid member dead-end tower

4.5.4 Pushover Analysis

Figure 4.17 shows the pushover curve (blue line) for the strengthened hybrid member dead-end tower. Furthermore, the corresponding pushover curves of the initial tower and the corroded model (Figure 4.12) are presented for comparison.

Pushover curves show that strengthening the diagonal members of the "vulnerable segment" (Segment 4) of the corroded dead-end tower slightly increases the strength of the corroded tower (i.e. the LF at which first failure occurs) but it is not enough to reach the strength of the initial tower (black line). In specific, for the strengthened hybrid tower the first failure occurs at *LF=11.63*. This value is between the corresponding values of the corroded tower (*LF=11.22*) and the initial tower (*LF=12.23*). It is noteworthy that all the other strengthening scenarios did not provide a much different value for the *LF* of the first failure. Thus, considering also the cost of strengthening, strengthening only the diagonal members of Segment 4 was the selected intervention.

Figure 4.17: Pushover curves of the initial, corroded and strengthened hybrid member dead-end tower

4.5.5 Dynamic Analysis

Figure 4.18 presents the typical results of the dynamic analyses regarding the top displacements in the transverse direction of the line (along Y). The time history of the graph at the left corresponds to a wind time history (input of analysis) with mean wind speed equal to 25 m/s at 10m (i.e. basic wind speed) and wind angle transverse to the direction of the line assuming no ice conditions. On the other hand, the graph at the right corresponds to exactly the same time history of wind but assuming an ice layer of 10mm thickness accredited on the tower members, insulators and conductors. The dynamic load was applied gradually during the first 30sec of the time history. In both cases the resulting top displacements were much lower than the failure limit from pushover for the strengthened hybrid member dead-end tower (Figure 4.17) and thus no failure was observed. Moreover, one could infer that a wind speed much larger than the basic wind speed of design is needed in order to observe a failure. Indeed, even for a time history with mean wind speed of 55m/s as in Figure 4.19, the dead-end tower is expected to fail only when 10mm ice will be accreted on the tower members and the conductors. The above findings are consistent with those of the cases of the initial and the corroded towers.

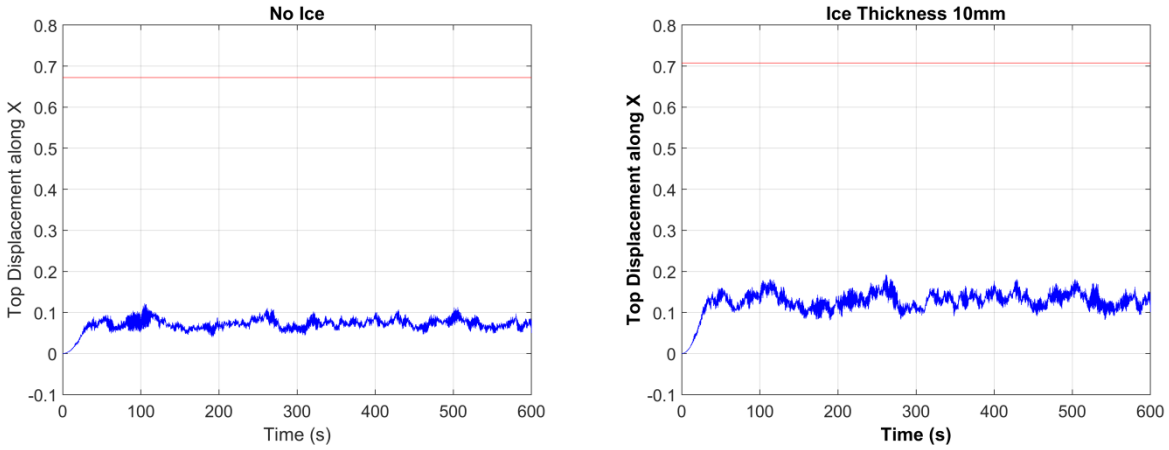

Figure 4.18: Typical time histories of top displacement in the transverse direction (along Y) of the strengthened hybrid dead-end tower for mean wind speed equal to the basic wind speed (25 m/s)

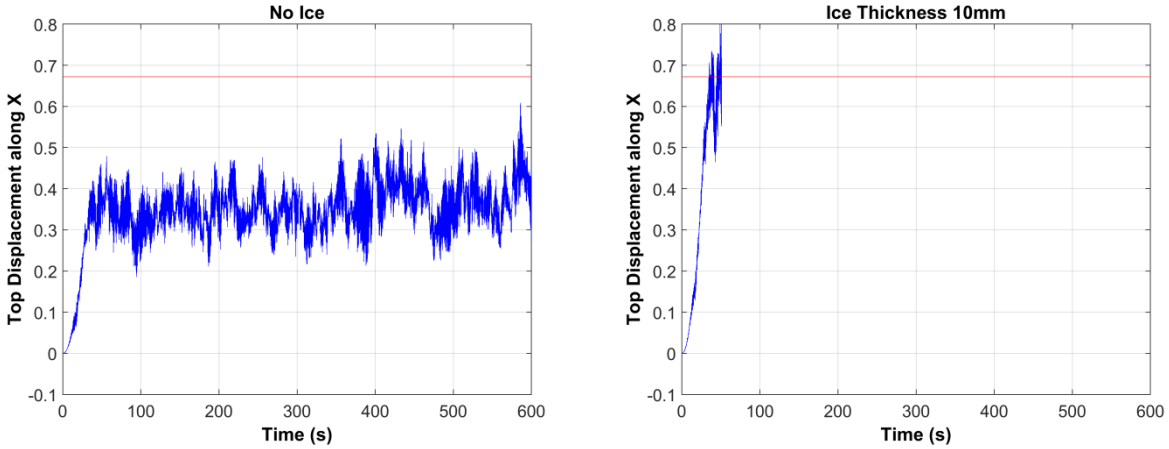

Figure 4.19: Time histories of top displacement in the transverse direction (along Y) of the strengthened hybrid dead-end tower for a mean wind speed of 55 m/s

4.6 High Strength Steel member Tower

4.6.1 Redesign with High Strength Steel

A redesigned version of the initial dead-end tower model with High Strength Steel (HSS) was also studied. The HSS tower had the same geometry with the initial one (Figure 4.1). Furthermore, two different grades were assumed with the corresponding actual values for yielding and ultimate stresses adopted by [2]. The angle profiles along with the corresponding steel grade for each of the group of members used in the HSS suspension tower are listed in Table 4.5. Finally, the use of HSS steel angle profiles reduced the total weight of the structure by 10.0 tons.

Table 4.5: Angle profiles used for the members of the HSS dead-end tower

Group	Angle Type	Angle Size	Steel grade
Bottom-legs	DAE	AM 300x300x28	S460M
Segment 2	DAE	AM 300x300x28	S460M
Segment 3	SAE	AM 250x250x34	S460M
Segment 4	SAE	AM 150x150x16-/+	S460M
Segment 5	SAE	AM 130x130x14	S460M
Segment 6	SAE	AM 75x75x6-	S460M
Segment 7	SAE	AM 65x65x4	S460M
Diagonal 1	SAE	AM 150x150x10-/+	S355J2
Diagonal 2	SAE	AM 140x140x12	S355J2
Diagonal 3	SAE	AM 180x180x13+	S355J2
Diagonal 4	SAE	AM 120x120x8	S355J2
Diagonal 5	SAE	AM 130x130x8	S355J2
Diagonal 6	SAE	AM 55x55x4	S355J2
Cross 1-bottom	SAE	AM 250x250x17	S460M
Cross 1-top	SAE	AM 120x120x7	S460M
Cross 1-base	SAE	AM 150x150x12-/+	S460M
Horizontal 1	SAE	AM 90x90x5	S460M
Horizontal 2	SAE	AM 130x130x9	S460M
Horizontal 3	SAE	AM 140x140x15	S460M
Horizontal 4	SAE	AM 75x75x4	S460M
Horizontal 5	SAE	AM 120x120x13	S460M
Horizontal 6	SAE	AM 55x55x4	S460M
Horizontal 1 base	SAE	AM 76x76x4.8	S460M
Horizontal 2 base	SAE	AM 80x80x5	S460M
Horizontal 3 base	SAE	AM 110x110x9	S460M
Horizontal 4 base	SAE	AM 90x90x7-	S460M
Cross - Horizontal	SAE	AM 75x75x7	S355J2
Cross 2-bottom	SAE	AM 180x180x13+	S460M
Cross 2-top	SAE	AM 90x90x5	S460M
Cross 2-base	SAE	AM 130x130x9	S460M
Redundant 1	SAE	AM 90x90x5	S355J2
Redundant 2	SAE	AM 100x100x6	S355J2
Redundant 3	SAE	AM 90x90x5	S355J2

4.6.2 Eigenvalue Analysis

Figure 4.20 presents the first three modes and the corresponding periods of the HSS tower assuming no ice accretion. The values of the eigenperiods are higher than the corresponding values of the initial model indicating that the use of HSS results in a less stiff structure than the initial model.

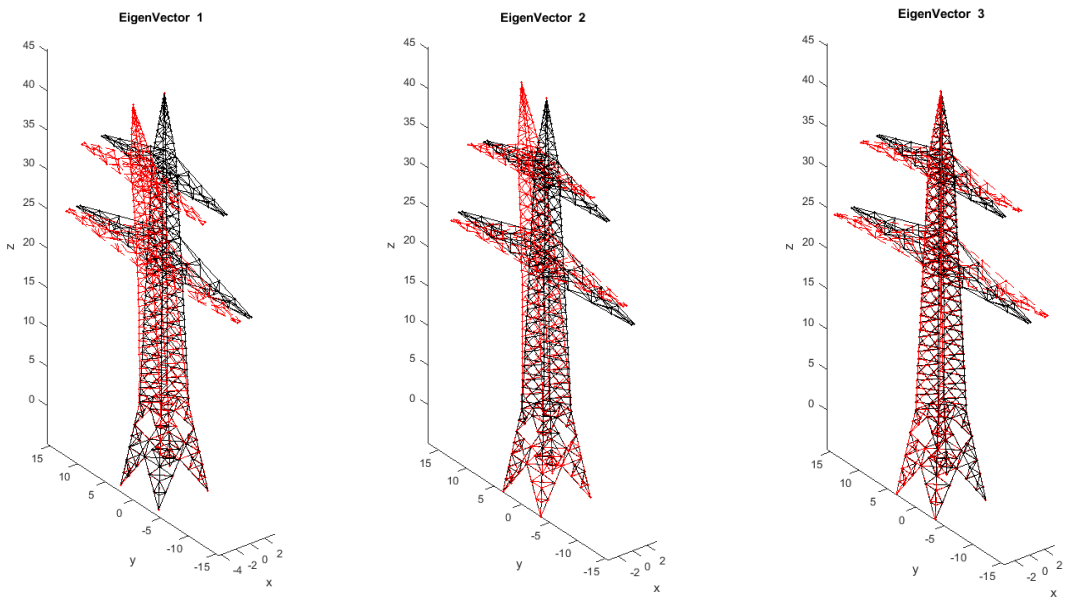

1st Mode
T_1=0.400 sec

2nd Mode
T_2=0.398 sec

3rd Mode
T_3=0.369 sec

Figure 4.20: First three modes and corresponding natural periods of the HSS dead-end tower

4.6.3 Pushover Analysis

Figure 4.21 shows the pushover curve (blue line) for the HSS suspension tower. Furthermore, the corresponding pushover curves of the initial and the corroded version of the tower are presented for the sake of comparison.

The curves follow the same pattern with those of the suspension tower (Figure 3.14). In specific, the *LF* when the first failure occurs is slightly lower than that of the initial model and the top displacement at the time of first failure is larger than any of the other models and equal 0.865m.

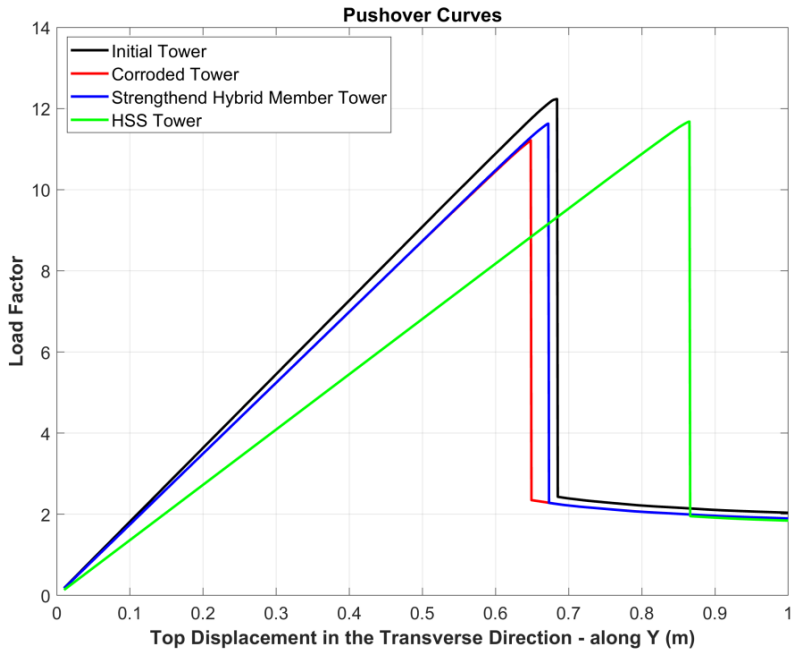

Figure 4.21: Pushover curves of the four versions of dead-end transmission towers

4.6.4 Dynamic Analysis

Figure 4.22 presents the typical results of the dynamic analyses regarding the top displacements in the transverse direction of the line (along Y). The time history of the graph at the left corresponds to a wind time history (input of analysis) with mean wind speed equal to 25 m/s at 10m (i.e. basic wind speed) and wind angle transverse to the direction of the line assuming no ice conditions. On the other hand, the graph at the right corresponds to exactly the same time history of wind but assuming an ice layer of 10mm thickness accredited on the tower members, insulators and conductors. The dynamic load was applied gradually during the first 30sec of the time history. In both cases the resulting top displacements were much lower than the failure limit from pushover for the HSS dead-end tower (Figure 4.21) and thus no failure was observed. Moreover, one could infer that a wind speed much larger than the basic wind speed of design is needed in order to observe a failure. Indeed, even for a time history with mean wind speed of 55m/s as in Figure 4.23, the dead-end tower is expected to fail only when 10mm ice will be accreted on the tower members and the conductors. The above findings are consistent with those of the cases of the initial, the corroded and the strengthened hybrid member towers.

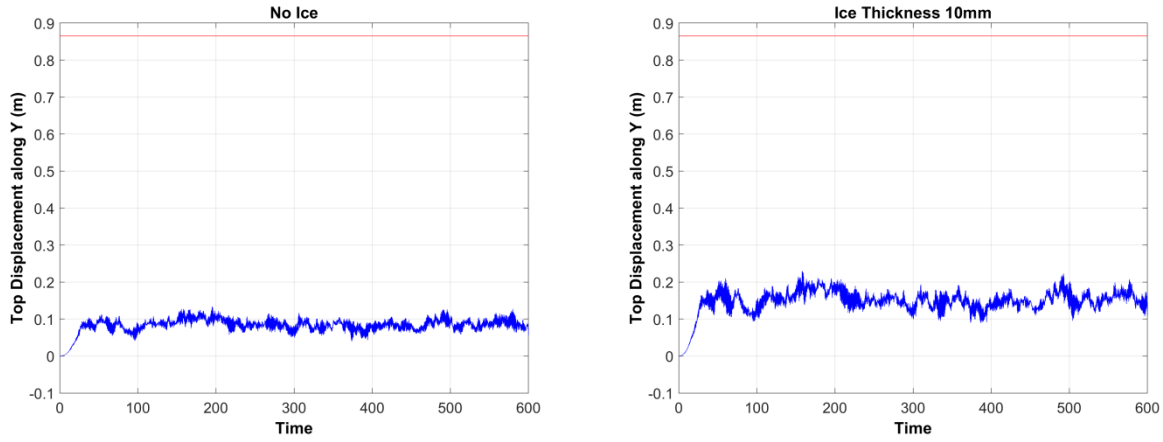

Figure 4.22: Typical time histories of top displacement in the transverse direction (along Y) of the HSS dead-end tower for mean wind speed equal to the basic wind speed (25 m/s)

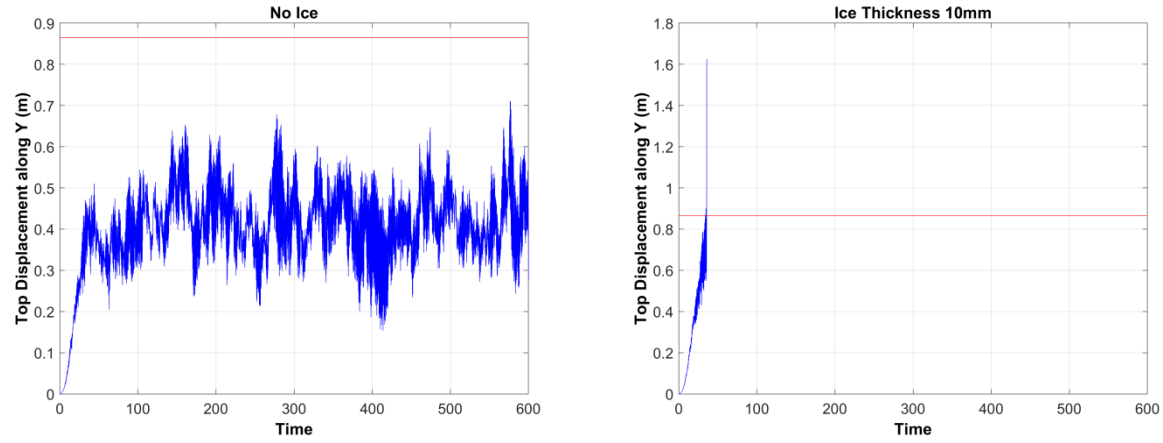

Figure 4.23: Time histories of top displacement in the transverse direction (along Y) of the HSS dead-end tower for a mean wind speed of 55 m/s

References

[1] ANGELHY Deliverable 1.3, Report on analysis and design of 6 case studies, Research Program of the Research Fund for Coal and Steel ANGELHY, Grant Agreement Number: 753993, European Commission, Brussels, Belgium, 2019.

[2] Braconi et al. Optimising the seismic performance of steel and steel-concrete structures by standardising material quality control (OPUS), Research Program of the Research Fund for Coal and Steel, Grant Agreement Number: RFSR-CT-2007-00039, European Commission, Brussels, Belgium, 2013.

[3] EN 1993-3-1, Design of steel structures. Part 3-1: Towers, masts and chimneys – Towers and masts. Brussels. Comité Europeen de Normalisation (CEN), 2006.

[4] Holmes J.D., Banks R.W., Roberts G., Drag and aerodynamic interference on microwave parabolic antennas and their supporting towers, Journal of Wind Engineering and Industrial Aerodynamics (50), 263-270, 1993.

[5] EN 1991-1-4, Design of steel structures. Part 1-4: General actions – Wind actions. Brussels. Comité Europeen de Normalisation (CEN), 2005.

[6] Holmes J.D. Wind loading of structures, Third Edition, CRC Press, Taylor & Francis Group, 2015.

[7] Martin P., Elena V.B., Loredo-Souza A.M., Camano E.B., Experimental study of the effects of parabolic antennas on the wind loading of telecommunication towers, Journal of Wind Engineering and Industrial Aerodynamics (149), 40-47, 2016.

[8] Carril C.F. Jr, Isyumov N., Brasil R.M.L.R.F., Experimental study of the wind forces on rectangular latticed communication towers with antennas, Journal of Wind Engineering and Industrial Aerodynamics (91), 1007-1022, 2003.

[9] IEC 61400-1. "Wind Turbines-Part 1: Design Requirements," International Electrotechnical Commission, Geneva, Switzerland, 2005.

[10] Jonkman B.J., Kilcher L., TurbSim User's Guide. Technical Report NREL/TP-xxx-xxxx (Draft Version). NREL Technical Report, National Renewable Energy Laboratory, Golden, Colorado, 2012.

[11] Taillon J.-Y., Legeron F., Prud'homme S., Variation of damping and stiffness of lattice towers with load level, Journal of Constructional Steel Research (71), 111-118, 2012.

[12] EN 12500:2000 Protection of metallic materials against corrosion – Corrosion likelihood in atmospheric environment – Classification, determination and estimation of corrosivity of atmospheric environments.

[13] EN ISO 9223. Corrosion of Metals and Alloys: Corrosivity of Atmospheres: Classification; European Committee for Standardization (CEN): Brussels, Belgium, 1992.

[14] EN ISO 9224. Corrosion of Metals and Alloys: Corrosivity of Atmospheres: Guiding Values for the Corrosivity Categories; European Committee for Standardization (CEN): Brussels, Belgium, 1992.

[15] EN ISO 9225. Corrosion of Metals and Alloys: Corrosivity of Atmospheres: Measurement of Pollution; European Committee for Standardization (CEN): Brussels, Belgium, 1992.

[16] EN ISO 9226. Corrosion of Metals and Alloys: Corrosivity of Atmospheres: Determination of Corrosion Rate of Standard Specimens for the Evaluation of Corrosivity; European Committee for Standardization (CEN): Brussels, Belgium, 1992.

[17] Landolfo R., Cascini L. Portioli, F., Modeling of metal structure corrosion damage: A state of the art report, Sustainability (2), 2163-2175, 2010.

[18] Knotkova D., Kreislova K., Corrosivity of atmospheres – derivation and use of information, WIT Transactions on State of the Art in Science and Engineering (28), 74-105, 2007.

[19] ANGELHY Deliverable 4.4, Design Guide, Research Program of the Research Fund for Coal and Steel ANGELHY, Grant Agreement Number: 753993, European Commission, Brussels, Belgium, 2020.

[20] Bezas, M.Z.; Tibolt, M.; Jaspart, J.-P.; Demonceau, J.-F., Critical assessment of the design of an electrical transmission tower. 9th International Conference on Steel and Aluminum Structures, 3-5 July 2019, Bradford, UK, 2019.

[21] Kiessling, F.; Nefger, P.; Nolasco, J.F.; Kaintzyk, U., Overhead Power Lines. New York: Springer, 2003.

[22] Cuchapin, J. (2018) Fundamental concepts of sag-tension relationship in transmission and distribution lines. Available online at: https://electricalengineerresources.com/2018/01/02/complete-sag-tension-relationship-in-transmission-and-distribution-lines-concepts/ (Accessed September 2019)

[23] Klinger, C.; Mehianpour, M.; Klingbeil, D.; Bettge, D.; Hacker, R.; Baer, W., Failure analysis on collapsed towers of overhead electrical lines in the region Münsterland (Germany) 2005. Engineering Failure Analysis (18), 1873-1883, 2011.

[24] Prasad Rao, N.; Samuel Knight, G.M.; Mohan, S.J.; Lakshmanan, N., Studies on failure of transmission line towers in testing. Engineering Structures (35), 55-70, 2012.

[25] Veletsos, A.S.; Darbre, G.R., Dynamic stiffness of parabolic cables, Earthquake Engineering and Structural Dynamics (11), 367-401, 1983.

List of Figures

List of Tables